Изучение столкновений тяжелых ионов на NICA

В. Рябов

NICA Project

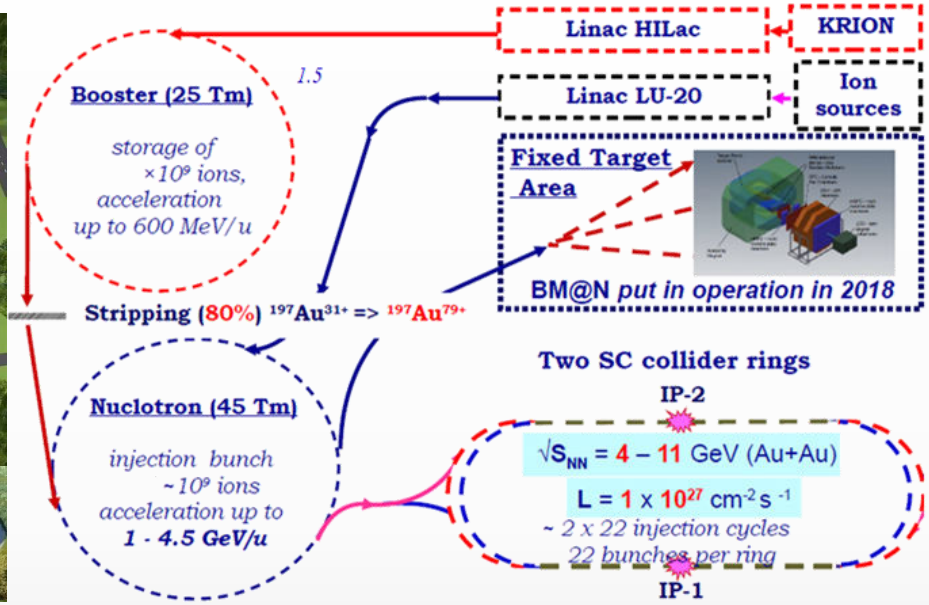

- The first megascience project in Russia, which is approaching its full commissioning:
  - ✓ already running in the fixed-target mode – BM@N
  - ✓ start of operation in collider mode in 2025 – MPD and later SPD
- Expected beam configuration in Stage-I:
  - ✓ Xe+Xe, Bi+Bi at $\sqrt{s_{NN}}$ = 4-11 GeV
  - ✓ heavy-ion beam luminosity up to ~10^{27} → collision rate ~ 5 kHz

System evolution in heavy-ion collisions

Fireball is ~10^{-15} meters across and lives for 5×10^{-23} seconds

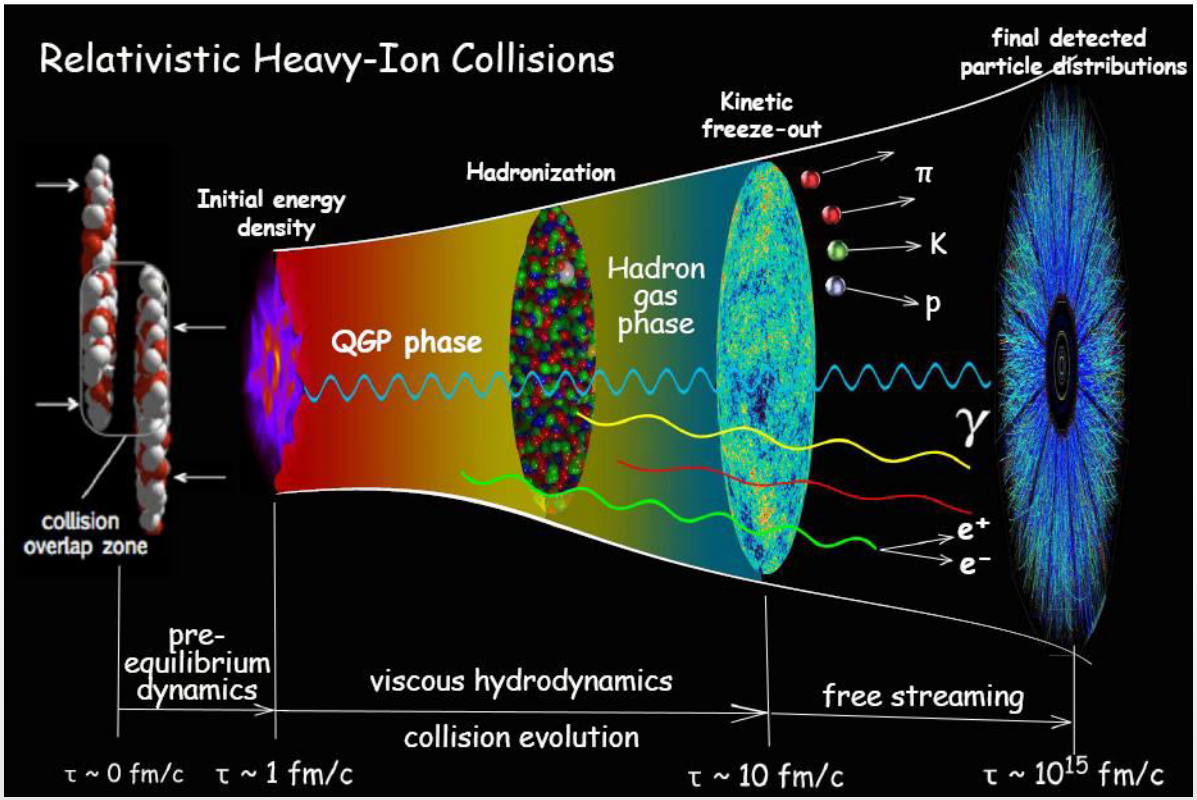

- The measurements are used to infer properties of the early state of relativistic heavy-ion collisions
- Only final state particles are measured in the detector: γ, $e^{\pm}$, $\mu^{\pm}$, π^0, $\pi^{\pm}$, K^0, $K^{\pm}$, η, ω, p, $\bar{p}$, ϕ, Λ, Σ, Ξ, etc.
- The measurements are used to infer properties of the early state of relativistic heavy-ion collisions

Particle detection

- Only particles that interact with the detector materials or decay in particles that interact can be detected
- Four known fundamental forces: Gravity, Weak, Electromagnetic and Strong interactions:
  - ✓ pions, protons: strong, electromagnetic
  - ✓ photons, electrons, muons: electromagnetic
- Particle decays:
  - ✓ strong and electromagnetic decays → very small lifetimes, ~ 10^{-23} s → decay daughters are undistinguishable from primaries:
    $\pi^0(\eta) \to \gamma\gamma$, $\omega(\eta) \to \pi^0\gamma$ ($\pi^0\pi^+\pi^-$), $\rho \to \pi\pi$, $K^* \to \pi K$, $\phi \to KK$, etc.
  - ✓ weak decays → long lifetimes, ~ 10^{-10} s → secondary decay vertices can be separated:
    $K_s^0 \to \pi^0\pi^0$, $K^\pm \to \mu\nu$, $\Lambda \to p\pi$, $\Sigma \to N\pi$, $\Omega \to \Lambda K$, etc.
- Detection of particles relies on the way particles (or daughters) interact with the materials:
  - ✓ track reconstruction in magnetic spectrometers → nondestructive method (particle remains): coordinates, momentum
  - ✓ calorimetric measurement of particle energy → destructive method (particle disappears): energy, coordinates
- Particle identification is an important ingredient of particle detection:
  - ✓ species dependent ionization losses: dE/dx vs. momentum
  - ✓ species dependent time of flight: Tof vs. momentum
  - ✓ species dependent shape of electromagnetic showers in the calorimeter: showers started by γ, $e^\pm$ and hadrons differ
  - ✓ species dependent penetration depth: $\mu^\pm$ can traverse a much larger width of material compared to other charged particles
  - ✓ species dependent threshold for Cherenkov/Transition radiation

Charged particle tracking and momentum measurements

Magnetic field analysis

- Charged particles are bended in the external magnetic field

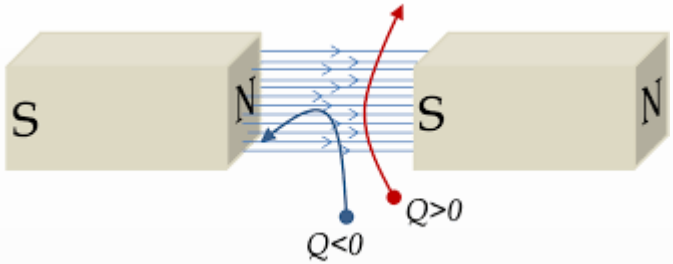

- The bending angle is related to particle momentum as p = q·B·R → for a fixed field B and particle charge q, the momentum p is proportional to the radius of curvature R
- Magnetic analysis is possible only for relatively long-lived particles to travel a measurable distance
- In nuclear physics, the relation becomes p [GeV/c] = 0.3 · B [T] · R [m] → a track with p = 1 GeV/c has a bending radius of R =1 m at B = 3T (magnetic field at the earth's surface is ~ $6 \cdot 10^{-5}$ T)
- Strong magnetic field and precise particle tracking can provide high resolution momentum measurements for long-lived charged particles
- Typical momentum resolution: $\delta p/p = \sqrt{c_1^2 + (c_2 p)^2}$ → less material and more precise tracking

$\delta p/p = c_1$ for multiple scattering $\delta p/p = c_2 p$ for position resolution

- Gaseous and semiconductor (not covered) detectors are most often used to reconstruct charged particle tracks in large active areas/volumes → non-destructive measurements

Ionization and drift in gases

❖ Charged particles produce ionization:

Gas	Density, mg cm^{-3}	E_x eV	E_I eV	W_I eV	$dE/dx\|_{min}$ keV cm^{-1}	N_P cm^{-1}	N_T cm^{-1}
H_2	0.084	10.8	13.6	37	0.34	5.2	9.2
He	0.179	19.8	24.6	41.3	0.32	3.5	8
Ne	0.839	16.7	21.6	37	1.45	13	40
Ar	1.66	11.6	15.7	26	2.53	25	97
Xe	5.495	8.4	12.1	22	6.87	41	312
CH_4	0.667	8.8	12.6	30	1.61	28	54
C_2H_6	1.26	8.2	11.5	26	2.91	48	112
iC_4H_{10}	2.49	6.5	10.6	26	5.67	90	220
CO_2	1.84	7.0	13.8	34	3.35	35	100
CF_4	3.78	10.0	16.0	35-52	6.38	52-63	120

W_I - average energy for creation of ion pair
N_T - total number of electron-ion pairs per cm

❖ External electric field → force movement of electrons and ions in the opposite directions:

- ✓ Electron drift velocity v_e = f(P, T, E, mixture) → by measuring drift time one can reconstruct a drift length → coordinates of ionization area
- ✓ Electron cloud diffuses as it drifts, diffusion ~ √L → dominates position resolution ~ √L D_T/√N
- ✓ Ion drift velocity v_i << v_e, linearly proportional to the electric field → can distort electric field configuration at high multiplicities/rates
- ✓ Gas mixtures are optimized for ionization density, drift velocity and spatial resolution (noble gases + quenchers)

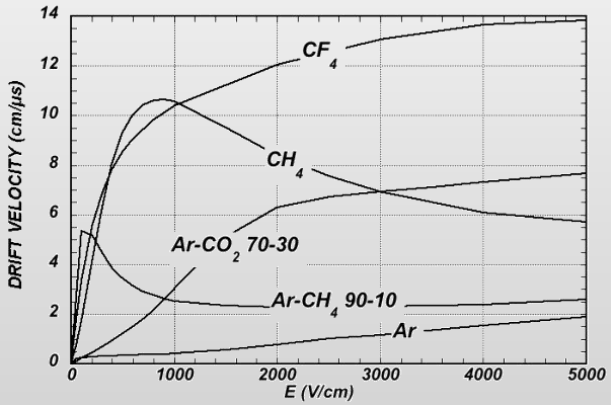

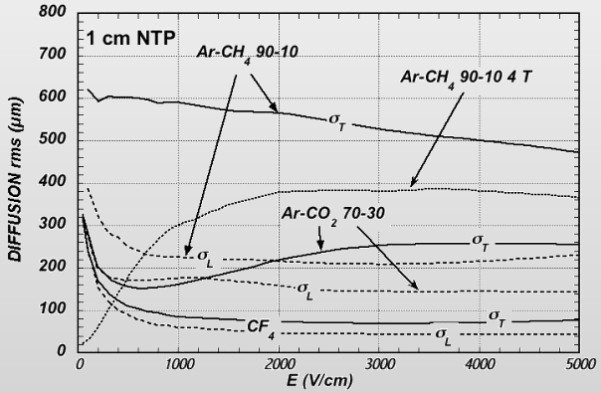

Ion mobility, v_i ~ μE

Gas	Mobility μ (cm^2 V^{-1} s^{-1})
He	10.4
Ne	4.7
Ar	1.54
Ar/CH_4	1.87
Ar/CO_2	1.72
CH_4	2.26
CO_2	1.09

Gas amplification

- If E >> 1 then electrons gain enough energy in a mean free path (λ) to ionize the gas
- $\alpha = 1/\lambda$ is the first Townsend coefficient
- Gas amplification (avalanche): $N = N_0 \cdot e^{\alpha x}$ in uniform electric field

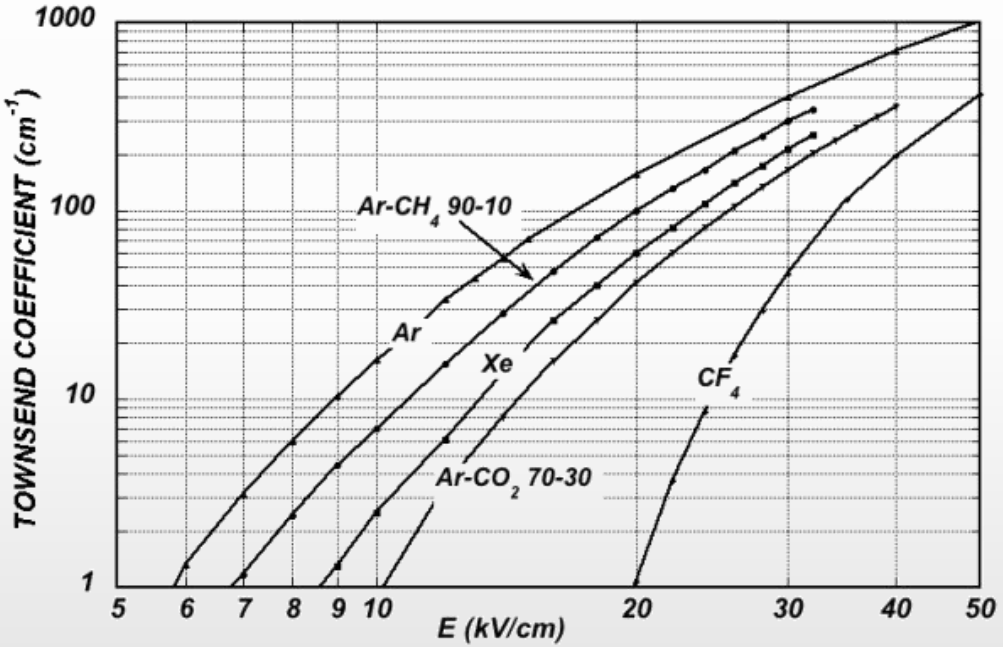

- Effective gas amplification starts at E > 20 kV/cm
- Large difference in threshold fields for entering the amplification regime for different gases
- Typical gas amplification in gaseous detectors ~ 10^4 to produce measurable signals

Gaseous trackers – Time Projection Chamber

❖ A typical Time Projection Chamber:

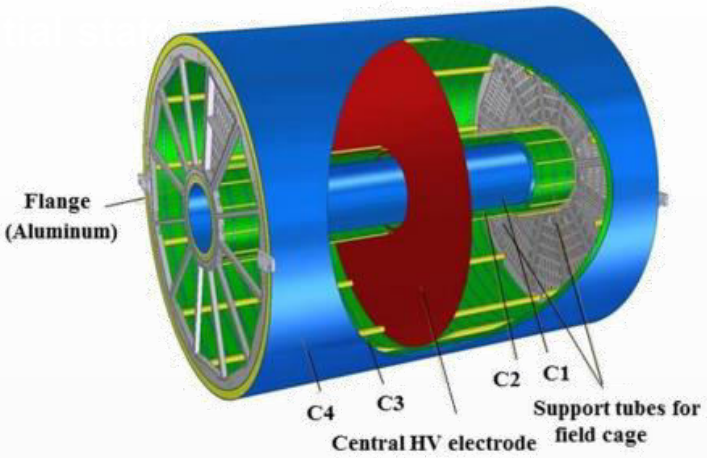

Item	Dimension
Length of the TPC	340 cm
Outer radius of vessel	140 cm
Inner radius of vessel	27 cm
Outer radius of the drift volume	133 cm
Inner radius of the drift volume	34 cm
Length of the drift volume	163 cm (of each half)
HV electrode	Membrane at the center of the TPC
Electric field strength	$\sim$ 140 V/cm
Magnetic field strength	0.5 Tesla
Drift gas	90% Ar+10% Methane, Atmospheric pres. + 2 mbar
Gas amplification factor	$\sim 10^4$
Drift velocity	5.45 cm/μs
Drift time	< 30 μs

- ✓ A large volume detector: $|\Delta\varphi| < 2\pi$, L ~ 350 m, $R_{i/o}$ ~ 30/150 cm
- ✓ Uniform electric field is formed by the central membrane (~ 30 kV) and voltage dividers on the vessel walls / rods
- ✓ Charged particle produces electron-ion pairs along the path
- ✓ Electrons drift towards the side planes equipped with MWPC, v_e ~ 50 μm/ns → 150 cm drift in ~ 30 μs
- ✓ Reconstructed points in the MWPC produce 2D projection of track
- ✓ The measured drift time is converted to drift distance to add the third coordinate → 3D points along the tracks
- ✓ Up to 53 points are measured along the path → track reconstruction → magnetic field analysis → $\delta p/p = \sqrt{(1\%)^2 + (1\% \cdot p)^2}$
- ✓ Double track resolution ~ 1 cm

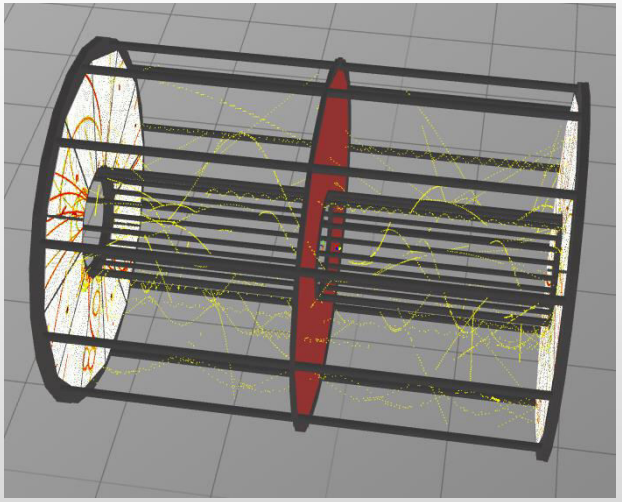

Application area of gaseous trackers

- Gaseous detectors are well suited to track charged particles in large active volumes (~ m^3)
  - ✓ high spatial resolution (~ 100 μm)
  - ✓ low material budget → minimize multiple scattering and photon conversion
  - ✓ sample many points along the track (10-200) → $\delta p/p \sim 1 - 2\ \%$
  - ✓ track hundreds and thousands of particles in a single event
  - ✓ small number of read-out channels (~ 10,000 - 100,000)
  - ✓ relatively cheap
  - ✓ PID by sampling particle dE/dx losses in the gas mixture

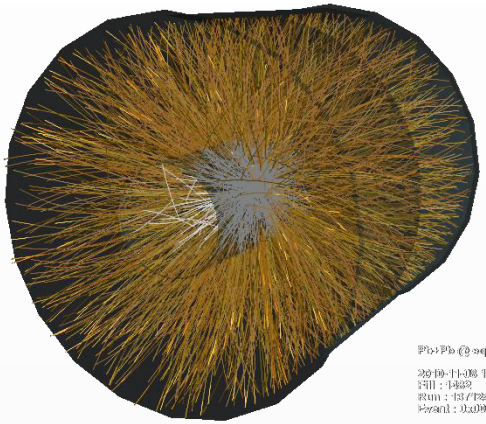

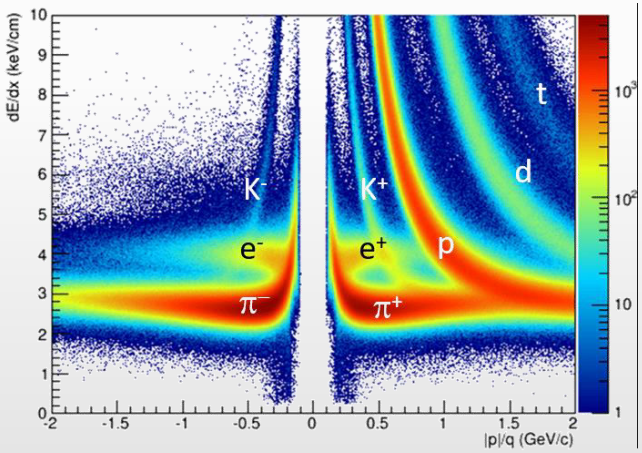

Bethe equation:

$$\left\langle -\frac{dE}{dx} \right\rangle = Kz^2 \frac{Z}{A}\frac{1}{\beta^2}\left[\frac{1}{2}\ln\frac{2m_e c^2\beta^2\gamma^2 W_{\max}}{I^2} - \beta^2 - \frac{\delta(\beta\gamma)}{2}\right]$$

valid at $0.1 < \beta < 1000$ within a few percent

- ✓ z, β - charge and velocity of incident particle
- ✓ Z, A – atomic number and atomic mass of absorber
- ✓ W_{max} – maximum passible energy transfer
- ✓ I – mean excitation energy
- ✓ $\delta(\beta\gamma)$ - density effect correction

Stopping power in a given material is a function of beta alone

- Limitations:
  - ✓ relatively low event rate ~ 10-100 kHz
  - ✓ double track resolution of ~ 1 cm prevents effective tracking close to the event vertex
  - ✓ subject to ageing at high radiation loads

Calorimetry

Calorimeters

- Measure particle full energy → particle is absorbed → destructive method
- Vary by purpose → hadronic (not covered) and electromagnetic calorimeters
- Construction details:
  - ✓ Absorb full particle energy and be compact → materials with small radiation length (X_0), $E = E_0 \cdot e^{-L/X0}$

Material	X_0 [cm]	ρ_M [cm]	E_c [MeV]
Fe	1.76	1.77	21–27
Pb	0.56	1.60	7.4
U	0.32	1.00	6.8
W	0.35	0.92	8
Polystyrol	42.9	8.25	80–109
Ar	14	7.2	41.7
Si	9.36	5.28	37.6
BGO	1.12	2.33	10.2
H_2O	36.10	10.9	70

Electromagnetic calorimeter depth: 15-30 X_0
Hadronic calorimeter depth: 5-8 nuclear integration lengths

  - ✓ Not all absorbing material can provide signals → possible solutions:
    - crystal calorimeters (CsI, PbGl, $PbWO_4$) → best precision, very expensive
    - sampling calorimeters → bricks of absorber (Pb) and read-out materials (Sc) via WLS fibers

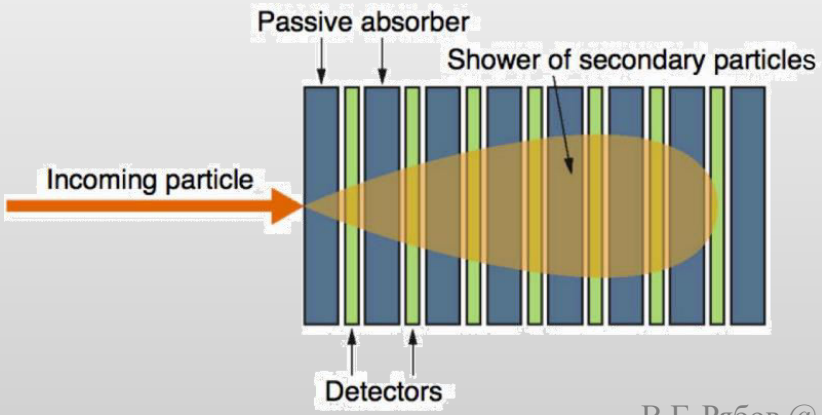

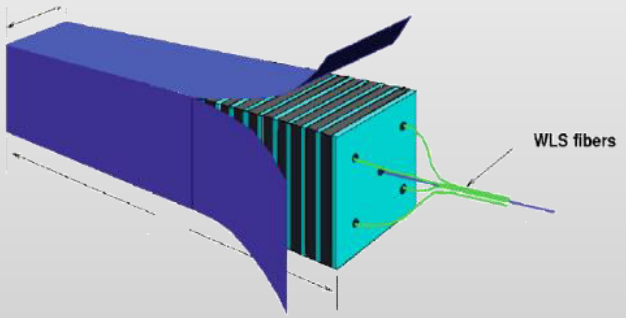

Calorimeter energy/spatial resolution

- The energy resolution of a calorimeter can be parameterized using:

$$\delta E/E = \sqrt{c_1^2 + \left(\frac{c_2}{\sqrt{E}}\right)^2 + \left(\frac{c_3}{E}\right)^2}$$

calibration term $\delta E/E \sim$ const

statistical term $\delta E/E \sim \delta N/N \sim 1/\sqrt{N} \sim 1/\sqrt{E}$

noise term $\delta E/E \sim const/E$

Constant term dominates energy resolution at high energy

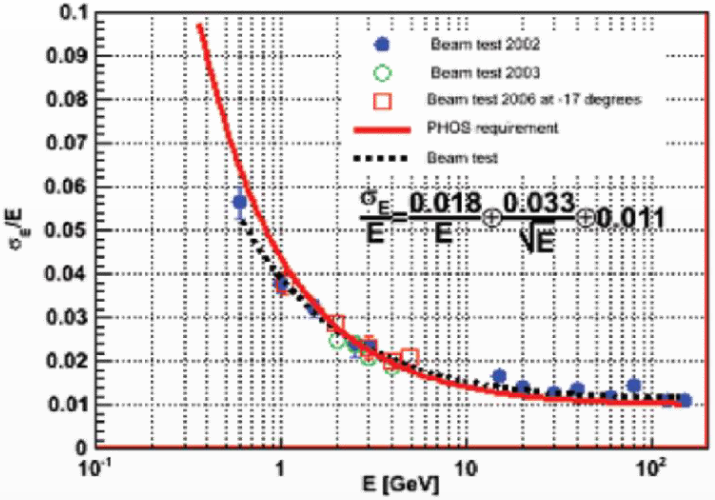

- Total signal is a sum of energies measured in several cells (towers) of the calorimeter → signal coordinates are weighted average of the tower coordinates

$$\bar{s} = \frac{\sum_{\text{digits}} s_i w_i}{\sum_{\text{digits}} w_i},$$

$$w_i = \max\left[0,\ p + \log\left(\frac{e_i}{E}\right)\right].$$

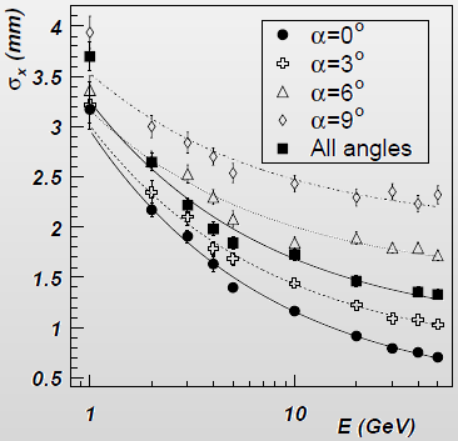

- ✓ Spatial resolution is inversely proportional to the measured energy, $\delta x/x = \sqrt{c_1 + \frac{c_2}{E}}$
- ✓ At E → 0, spatial resolution tends to a half-size of a single calorimeter cell

- Both energy and spatial resolutions degrade at large incident angles → projective geometry is preferable

Shower shapes

❖ Shape and size of the energy deposition region depends on the particle species and type of interaction

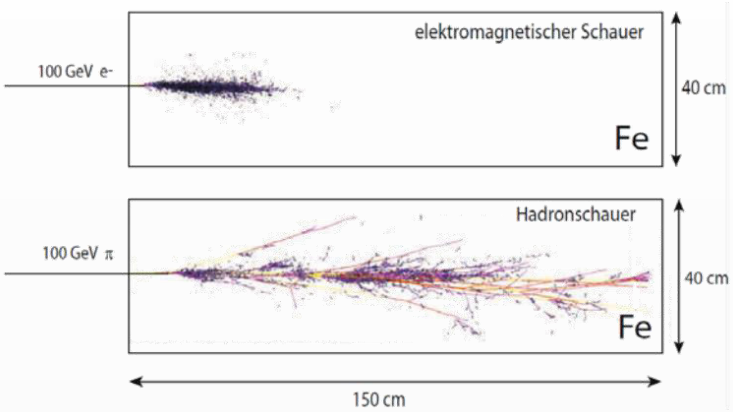

– Electromagnetic shower (γ, $e^{\pm}$)

– Production of mesons (π, K, …) and baryons (n, p, …)
– Spallation
– Excitation of nuclei
– Nuclear fission
– Photons from π^0 decays initiate new electromagnetic showers

❖ Shape of the electromagnetic shower can be measured ($e^{\pm}$ or photon beams) or simulated

❖ By comparing the measured and expected shower shapes one can discriminate between hadronic and electromagnetic showers → particle identification / hadron suppression:

$\mathrm{Chi2} = \sum_i \frac{\left(E_i^{measured} - E_i^{expected}\right)^2}{\sigma_i^2}$, where: $E_i^{expected}$ is calculated for each tower based on the known shower shape, σ_i^2 is expected fluctuation of the energy distribution (empirical tuning), NDF – number of towers in the shower

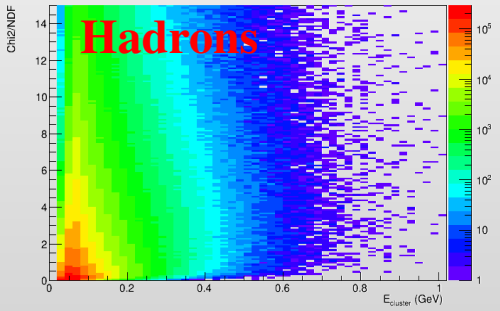

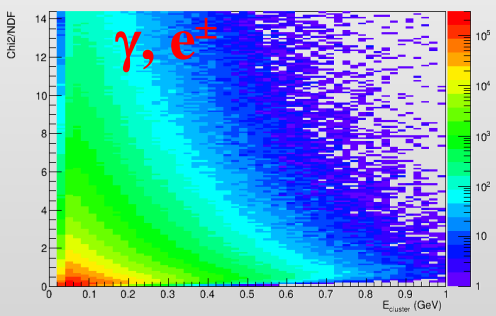

✓ shower shapes are different for (γ, $e^{\pm}$) and hadrons

✓ shower shape analysis is possible for showers with number of towers > 1

✓ provides capabilities for rejection of hadronic signals in the measurements for γ and $e^{\pm}$ → particle identification

Particle identification by velocity

Particle identification by time-of-flight (tof)

- Charged particle track is reconstructed in the tracking detector → magnetic analysis → momentum p
- Reconstructed track can be extrapolated to outer detector walls and matched to the measured hits
- Time of flight measurements are possible with fast detectors (MRPC, Micro channel plate detectors …)

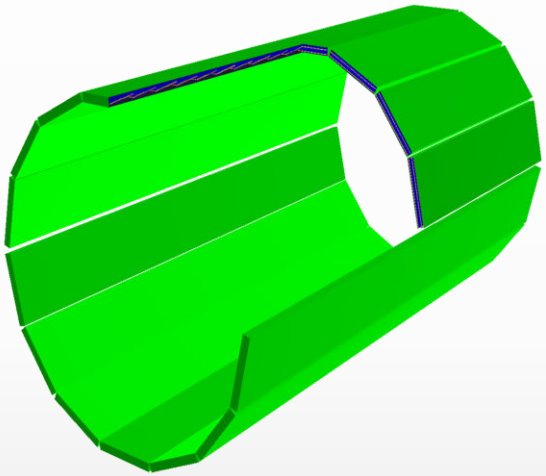

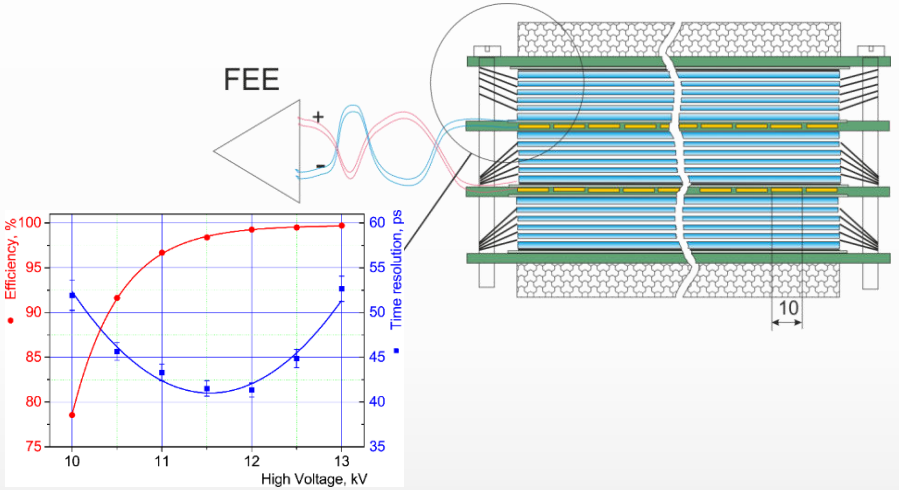

- Square of particle mass and the resolution are defined as:

$$m^2 = p^2\left(\frac{t^2c^2}{L^2} - 1\right) \qquad \delta^2_{m^2} = 4m^4\frac{(\delta p)^2}{p^2} + 4p^4\frac{tc}{L}\frac{(\delta t)^2}{t}$$

→ depends both on momentum and tof resolution
→ second term is inversely proportional to flight path L

- With momentum resolution of $\frac{\delta p}{p} \sim 1\%$ and $\delta t \sim 100$ ps charged hadrons are separated up to a few GeV/c

Complementary measurements

- Combined measurements of dE/dx and tof provide hadron separation in a wide momentum range:
  - ✓ tracker provides PID signals for all reconstructed tracks, including those with momentum → 0
  - ✓ TOF walls located at larger radii do not detect low-momentum particles (bend in the magnetic field)
- Both measurements are based on particle separation by velocity
- Particle separation from ~zero up to ~ 3 GeV/c

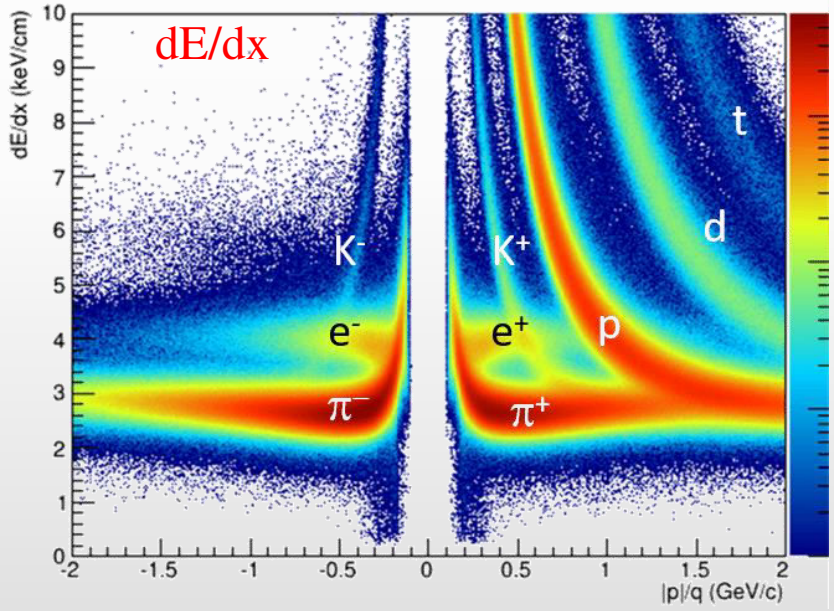

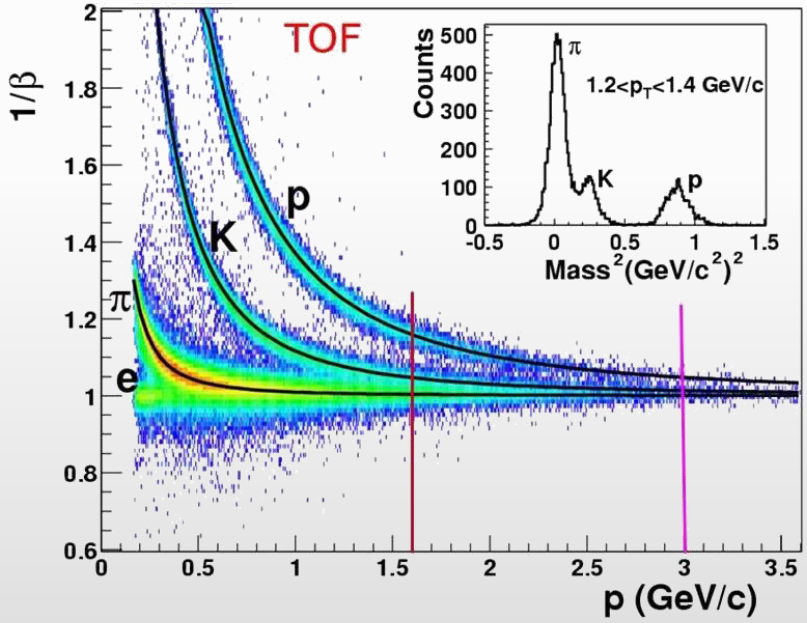

Heavy ion collisions at NICA

Operation details

- Relatively low collision energies (4-11 GeV):
  - ✓ modest multiplicity (~ 1000 particles per event)
    → modest track density even close to event vertex
  - ✓ bulk of particles is produced at low momentum ($\langle p_T \rangle$ ~ 100-300 MeV/c for light-flavor hadrons)
    → no need for a very strong magnetic field and high-momentum PID, minimization of multiple scattering
  - ✓ heavy flavor production cross section is small
    → topic needs special attention

- Top NICA luminosity for heavy-ion beams is 10^{27} $cm^{-1}s^{-1}$:
  - ✓ maximum event rate ~ 7 kHz
    → no need for very fast detectors

Multi-Purpose Detector

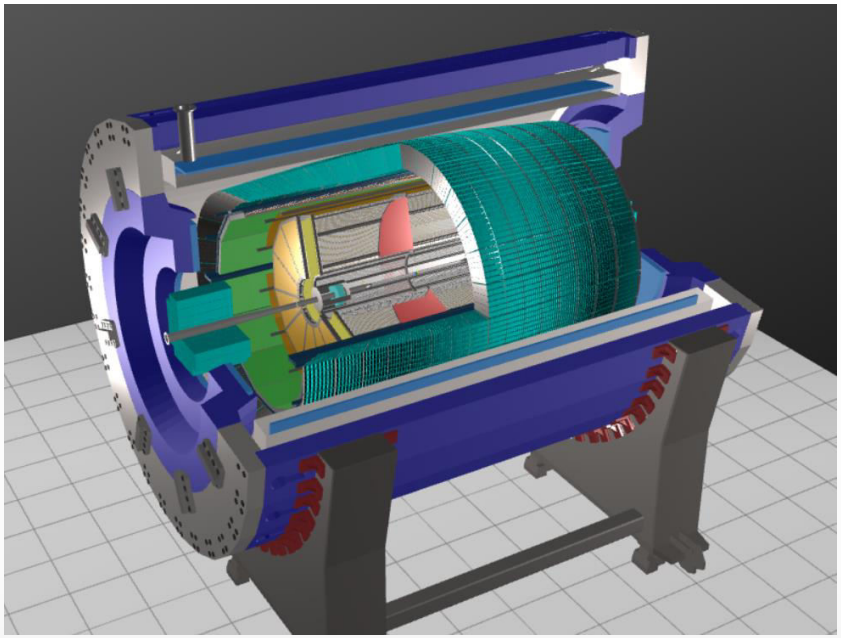

Length	340 cm
Vessel outer radius	140 cm
Vessel inner radius	27 cm
Default magnetic field	0.5 T
Drift gas mixture	90% Ar+10% CH_4
Maximum event rate	7 kHz ($L = 10^{27}$ $cm^{-2}s^{-1}$)

TPC: $|\Delta\varphi| < 2\pi$, $|\eta| \leq 1.6$
TOF, EMC: $|\Delta\varphi| < 2\pi$, $|\eta| \leq 1.4$
FFD: $|\Delta\varphi| < 2\pi$, $2.9 < |\eta| < 3.3$
FHCAL: $|\Delta\varphi| < 2\pi$, $2 < |\eta| < 5$

TPC: charged particle tracking + momentum measurements + identification by dE/dx
TOF: charged particle identification by m^2/β
EMC: energy and PID for $\gamma/e^{\pm}$ + charged particle identification (limited ability)
FFD/FHCAL: event triggering, event geometry, T_0
ITS: secondary vertex reconstruction for heavy-flavor decays (very small S/B ratio)

Charged particle tracking and PID

- Magnetic field ~ 0.5 T and up to 53 points measured along the track in the TPC:

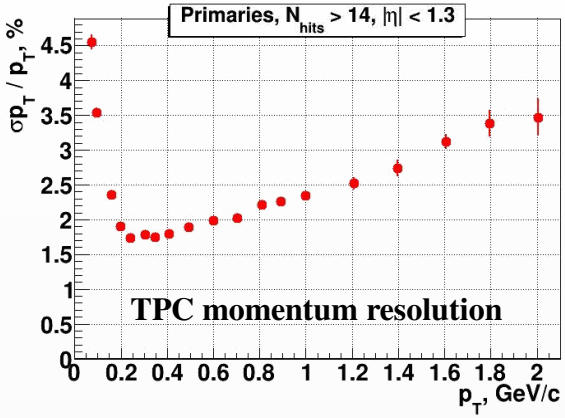

- PID by dE/dx (resolution ~6.5%) and tof (δt ~ 85 ps) → excellent light flavor hadron and fragment identification capabilities in a wide rapidity range

dE/dx vs momentum in TPC

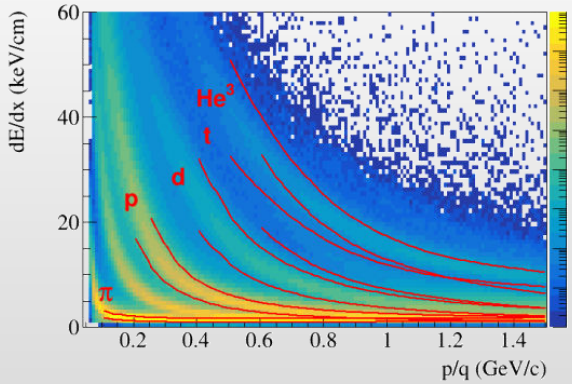

m^2 vs. momentum in TOF

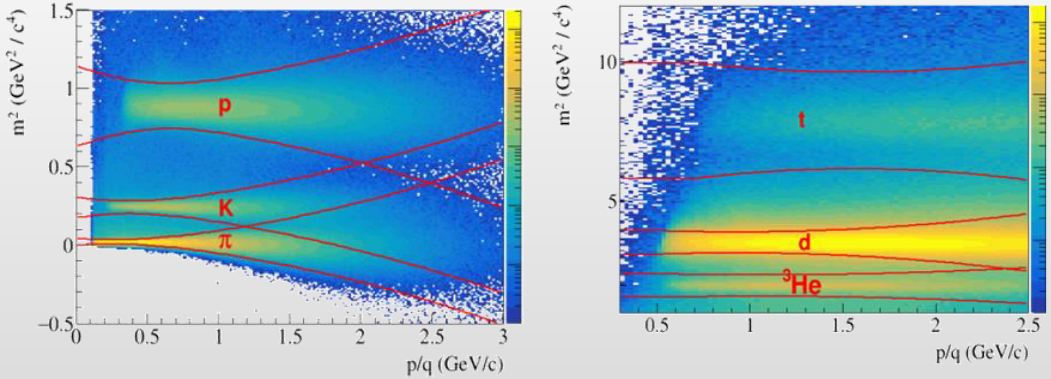

- Electron and photon measurements and identification in the ECAL

MPD detector

Eur.Phys.J.A 58 (2022) 7, 140

- For the MPD detector at NICA, well known detector technologies were selected to fulfill the requirements for the event rates and observables of interest at reasonable cost
- Relatively ‘simple’ design of the MPD detector provides high flexibility and physics potential
- The MPD detector is in final stage of production, commissioning and first data taking in 2025

Physics at NICA

Heavy-ion collisions

- QCD is a fundamental theory of strong interactions
- Only colorless particles are observed in the experiment (no free quarks or gluons) → confinement
- QGP is a state of matter in which quarks and gluons are free to move in space >> size of the nucleon
- QGP matter formation:

Two recipes:

(a) at high T - Early universe

(b) at high baryon density – Neutron stars

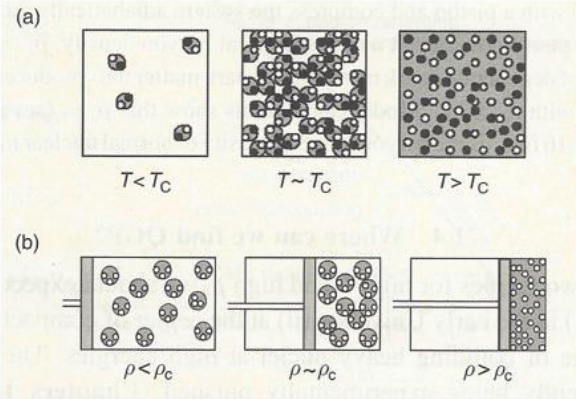

Relativistic heavy ion collisions - A combination of the two recipes

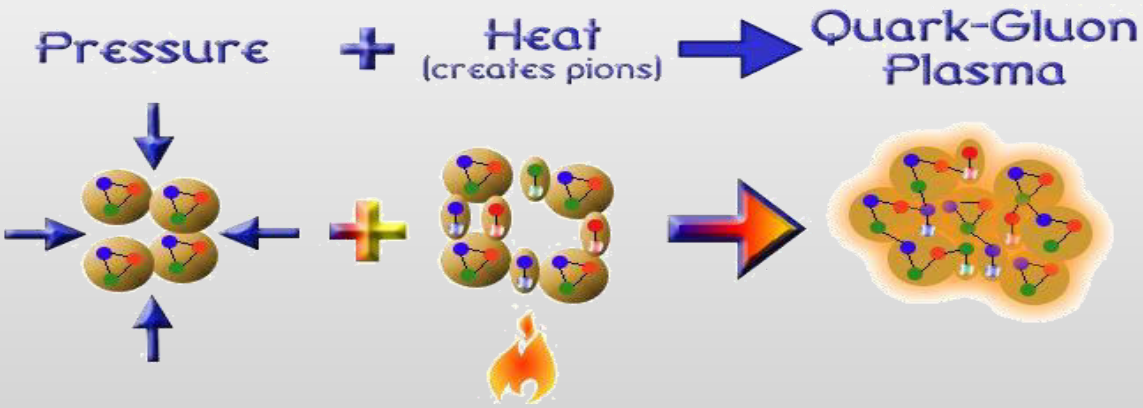

Coining of a name

Ed Shuryak - Physics Reports 1980

First review on QCD at extreme density conditions

"Because of the apparent analogy with similar phenomena in atomic physics, we may call this phase of matter the QCD (or quark-gluon) plasma."

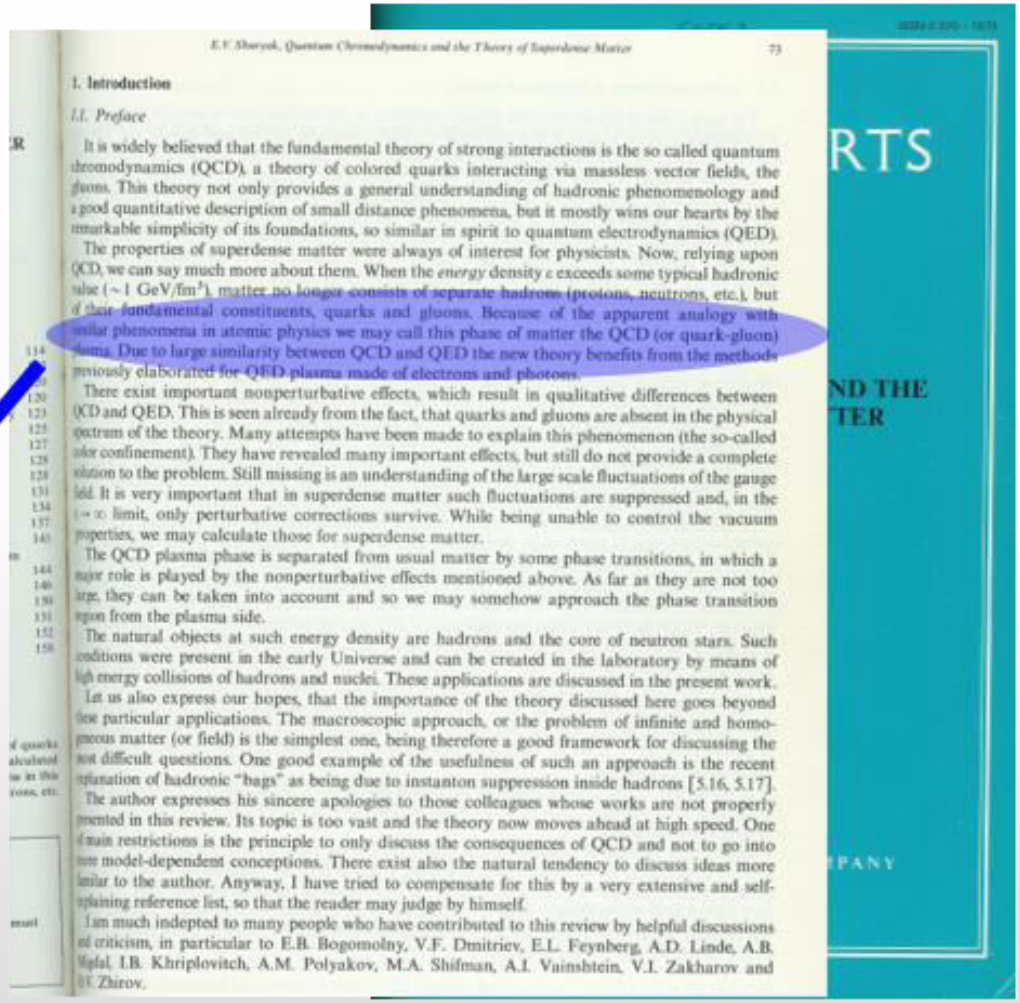

E.V. Shuryak, Quantum Chromodynamics and the Theory of Superdense Matter 73

1. Introduction

1.1. Preface

It is widely believed that the fundamental theory of strong interactions is the so called quantum chromodynamics (QCD), a theory of colored quarks interacting via massless vector fields, the gluons. This theory not only provides a general understanding of hadronic phenomenology and a good quantitative description of small distance phenomena, but it mostly wins our hearts by the remarkable simplicity of its foundations, so similar in spirit to quantum electrodynamics (QED).

The properties of superdense matter were always of interest for physicists. Now, relying upon QCD, we can say much more about them. When the *energy* density ε exceeds some typical hadronic value (~ 1 GeV/fm^3), matter no longer consists of separate hadrons (protons, neutrons, etc.), but of their fundamental constituents, quarks and gluons. Because of the apparent analogy with similar phenomena in atomic physics we may call this phase of matter the QCD (or quark-gluon) plasma. Due to large similarity between QCD and QED the new theory benefits from the methods previously elaborated for QED plasma made of electrons and photons.

There exist important nonperturbative effects, which result in qualitative differences between QCD and QED. This is seen already from the fact, that quarks and gluons are absent in the physical spectrum of the theory. Many attempts have been made to explain this phenomenon (the so-called color confinement). They have revealed many important effects, but still do not provide a complete solution to the problem. Still missing is an understanding of the large scale fluctuations of the gauge field. It is very important that in superdense matter such fluctuations are suppressed and, in the $\varepsilon \to \infty$ limit, only perturbative corrections survive. While being unable to control the vacuum properties, we may calculate those for superdense matter.

The QCD plasma phase is separated from usual matter by some phase transitions, in which a major role is played by the nonperturbative effects mentioned above. As far as they are not too large, they can be taken into account and so we may somehow approach the phase transition region from the plasma side.

The natural objects at such energy density are hadrons and the core of neutron stars. Such conditions were present in the early Universe and can be created in the laboratory by means of high energy collisions of hadrons and nuclei. These applications are discussed in the present work.

Let us also express our hopes, that the importance of the theory discussed here goes beyond these particular applications. The macroscopic approach, or the problem of infinite and homogeneous matter (or field) is the simplest one, being therefore a good framework for discussing the most difficult questions. One good example of the usefulness of such an approach is the recent explanation of hadronic "bags" as being due to instanton suppression inside hadrons [5.16, 5.17].

The author expresses his sincere apologies to those colleagues whose works are not properly presented in this review. Its topic is too vast and the theory now moves ahead at high speed. One of main restrictions is the principle to only discuss the consequences of QCD and not to go into too model-dependent conceptions. There exist also the natural tendency to discuss ideas more similar to the author. Anyway, I have tried to compensate for this by a very extensive and self-explaining reference list, so that the reader may judge by himself.

I am much indepted to many people who have contributed to this review by helpful discussions and criticism, in particular to E.B. Bogomolny, V.F. Dmitriev, E.L. Feynberg, A.D. Linde, A.B. Migdal, I.B. Khriplovitch, A.M. Polyakov, M.A. Shifman, A.I. Vainshtein, V.I. Zakharov and Ya.B. Zhirov.

LQCD calculations

- The QGP is predicted by numerical calculations of QCD on the lattice

Bazavov et al., PLB 795,15 (2019) PLB 478, 447 (2000)

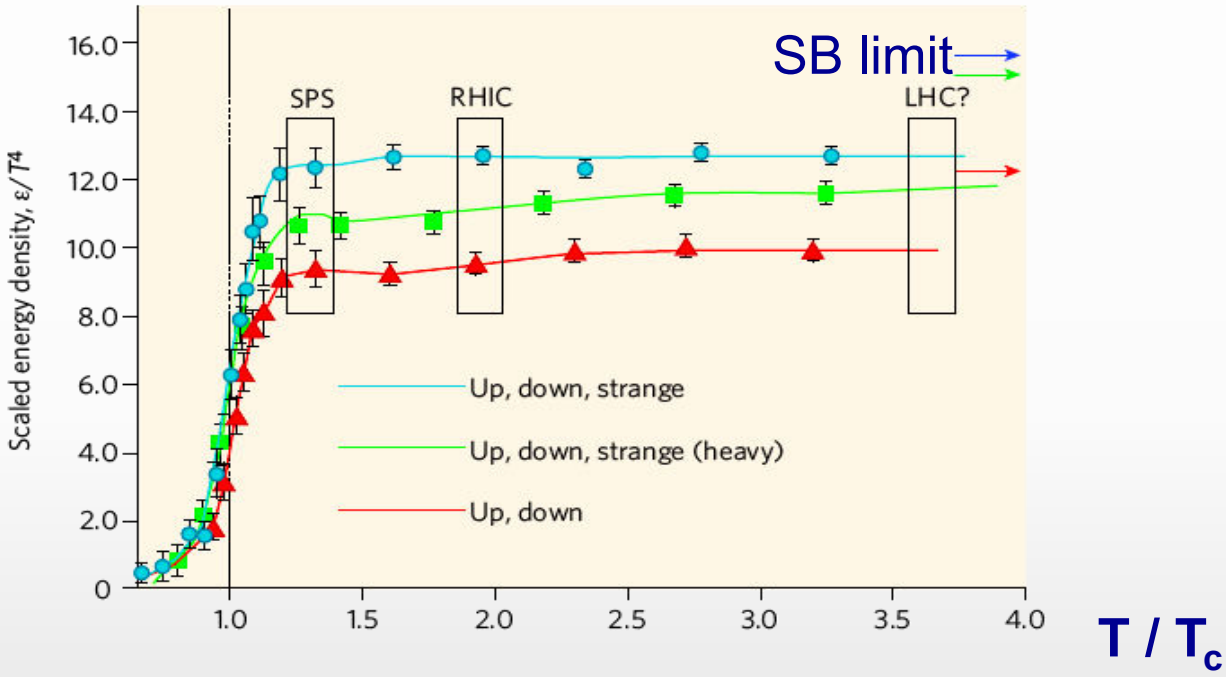

Recent LQCD calculations show that the critical temperature is: T_c (at $\mu_B = 0$) = 156.5 ± 1.5 MeV

- Fundamental characteristics of the QGP:
  - ✓ deconfinement → quasi-free quarks and gluons in a volume >> hadron size
  - ✓ chiral symmetry restoration → constituent quark mass ~ 300 MeV turns into current quark mass ~ 5-10 MeV

Heavy-ion collisions

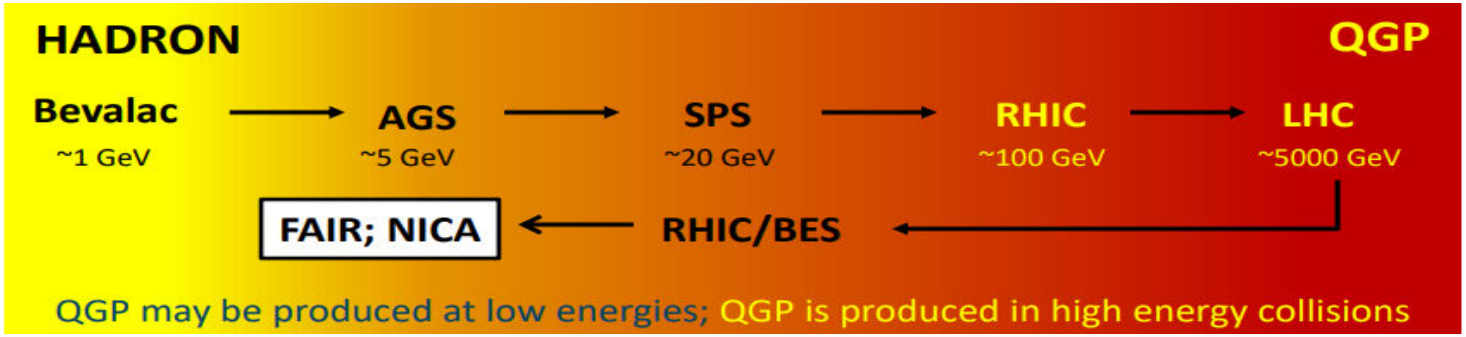

Short heavy-ion physics history

❖ **BEVALAC – LBNL** 1972-1984 max. $\sqrt{s_{NN}}$ = 2.2 GeV			
❖ **SPS – CERN** 1986-2000 $\sqrt{s_{NN}}$ = 17.3 GeV	NA35/49, NA44, NA38/50/51, NA45, NA52, NA57, NA60, WA80/98, WA97 …	Fixed target	
❖ **AGS – BNL** 1988-1996 $\sqrt{s_{NN}}$ = 4.8 GeV	E864/941, E802/859/866/917, E814/877, E858/878, E810/891, E896, E910 …		
❖ **SIS18 – GSI** 1990 → $\sqrt{s_{NN}}$ = 2.4 GeV			
❖ **RHIC – BNL** 2000-2025 $\sqrt{s_{NN}}$ = 200 GeV	BRAHMS, PHENIX, PHOBOS, STAR	Collider	
❖ **LHC – CERN** 2010 → $\sqrt{s_{NN}}$ = 5.02 TeV	ALICE, ATLAS, CMS, LHCb		

Near future

❖ NICA – JINR 2024 $\sqrt{s_{NN}}$ = 11 GeV	MPD, BM@N	Collider & Fixed target
❖ SIS100 – FAIR 2028? $\sqrt{s_{NN}}$ = 5 GeV	CBM, HADES	Fixed target

Heavy-ion collisions

- ❖ Study QCD under extreme conditions of temperature and density
- ❖ Explore the QCD phase diagram, search for the QGP and study its properties

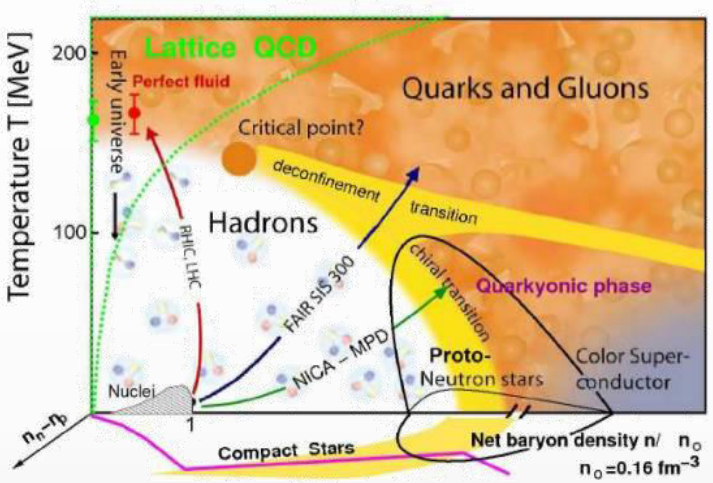

- ✓ Primordial form of QCD matter at high temperature and/or (net)baryon density
- ✓ Present during the first microseconds after Big Bang
- ✓ Provides an example of phase transitions which may occur at a variety of higher temperature scales in the early universe
- ✓ Provide important insights on the origin of mass for matter, and how quarks are confined into hadrons

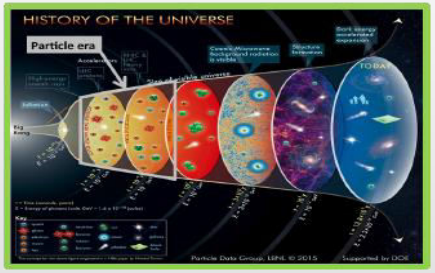

High temperature:
Early Universe evolution

High baryon density:
Inner structure of
compact stars

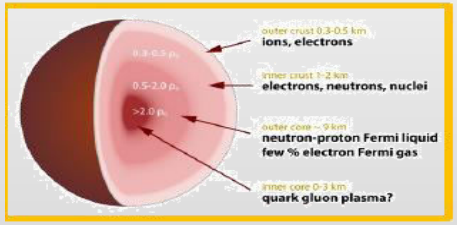

- ❖ At NICA, both BM@N and MPD study QCD medium at extreme net baryon densities

Mapping the QCD diagram

- Measurements of particle integrated yields are used to determine chemical freeze-out conditions
- In Statistical Model of Hadron Production (SHMP) where hadrons are emitted from the interaction region in statistical equilibrium abundancy (N_c) of particles with mass m and charge q, baryon number B and spin factor $g = 2s+1$ is defined as:

$$N_C = \frac{gV}{\pi^2} m^2 T K_2\left({}^{m}/_{T}\right) \exp\left(\frac{B\mu_B + q\mu_q}{T}\right) \text{, where} \qquad {}^{\mu_q}/_{T} = \frac{1}{2} ln \frac{\pi^+}{\pi^-}$$

- By measuring particle integrated yields one can determine T, μ_B and V as fit parameters

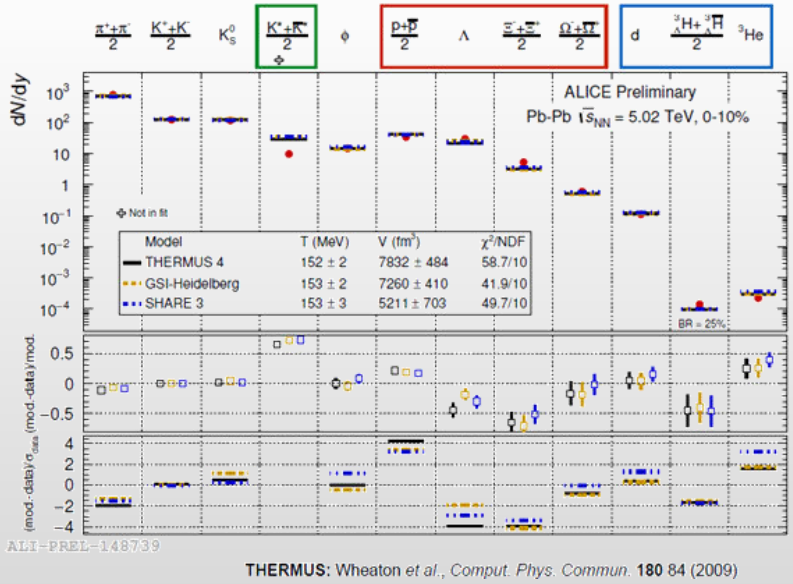

THERMUS: Wheaton *et al.*, *Comput. Phys. Commun.* **180** 84 (2009)

A. Andronic et al. Physi Lett B 673 (2009) 142 145 143

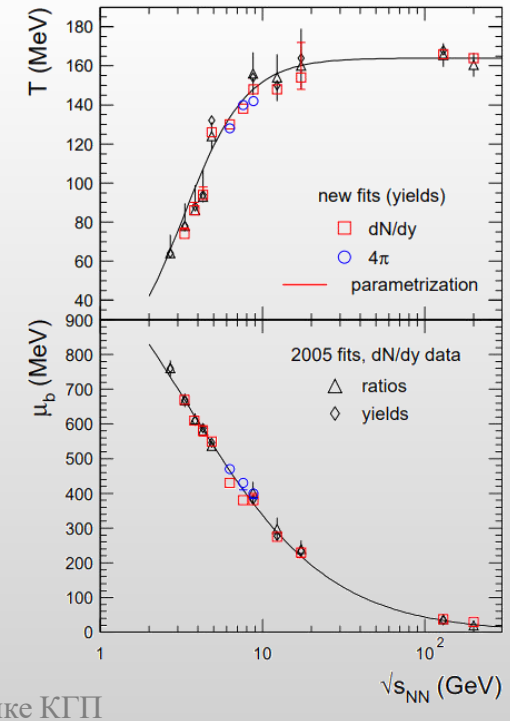

Mapping the kinetic freeze out conditions

- Particle transverse momentum spectra are used to determine kinetic freeze-out conditions
- A simplified hydrodynamic model with three fit parameters is used to describe particle production from a thermalized source + radial flow boost → Blast-Wave model:

  - ✓ T_{Kin}: kinetic freeze out temperature
  - ✓ $\langle\beta_T\rangle$: transverse radial flow velocity
  - ✓ n: velocity profile exponent

$$E\frac{d^3N}{dp^3} \propto \int_0^R m_T I_0\left(\frac{p_T \sinh(\rho)}{T_{Kin}}\right) K_1\left(\frac{m_T \cosh(\rho)}{T_{Kin}}\right) r\,dr$$

$$m_T = \sqrt{m^2 + p_T^2} \qquad \rho = \tanh^{-1}(\beta_T) \qquad \beta_T = \beta_s\left(\frac{r}{R}\right)^n$$

- Three parameters require simultaneous fit to the measured π, K, p, … etc. spectra:

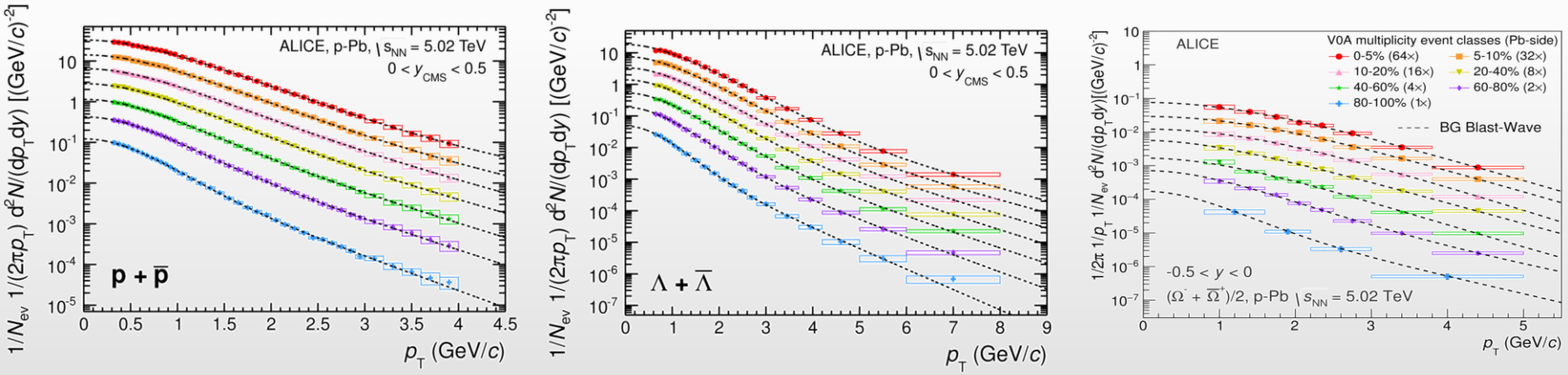

- p_T distributions for different particle species are well reproduced with a single set of fit parameters
- Mass- and centrality-dependent hardening of the spectra is well reproduced

Blast-wave model fits

- Fit results for pp, p-A and A-A collisions at LHC energies:

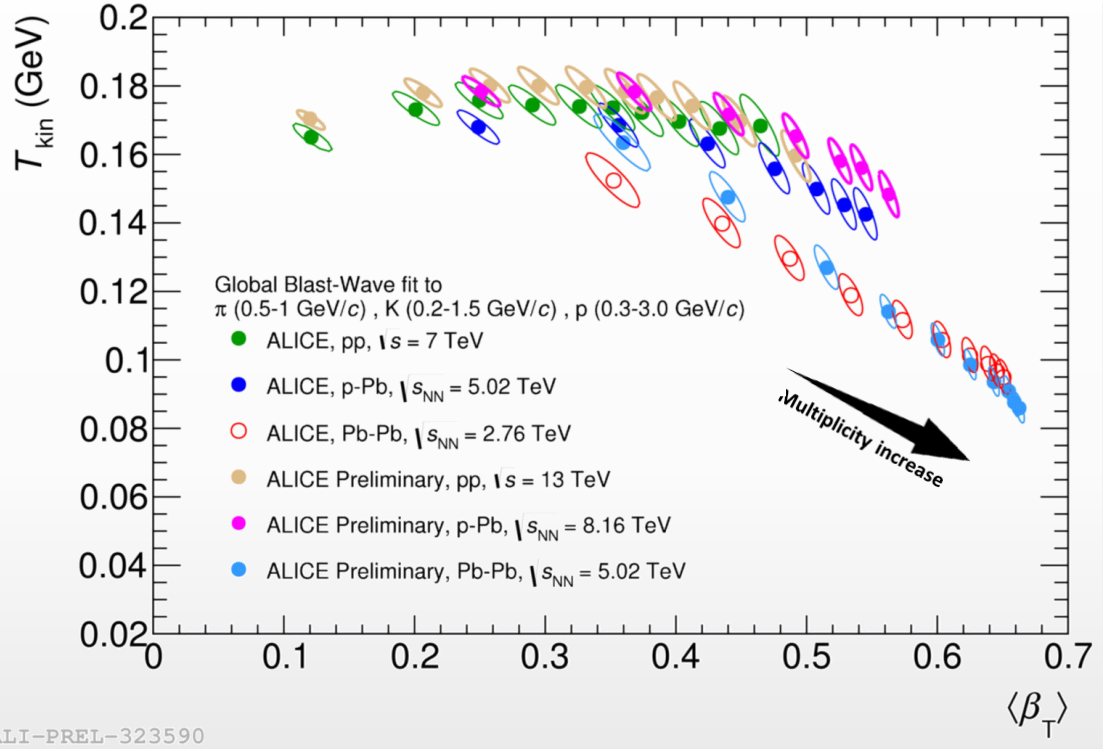

- Largest $\langle\beta_T\rangle$ and lowest T_{kin} for more central (higher-multiplicity) collisions
- pp/p-A: T_{kin} nearly constant for pp, small decrease in p-A; radial flow $\langle\beta_T\rangle$ increases with multiplicity
- A-A collisions show a different trend

Compilation of freeze out conditions

Phys. Rev. C 96, 044904 (2017)

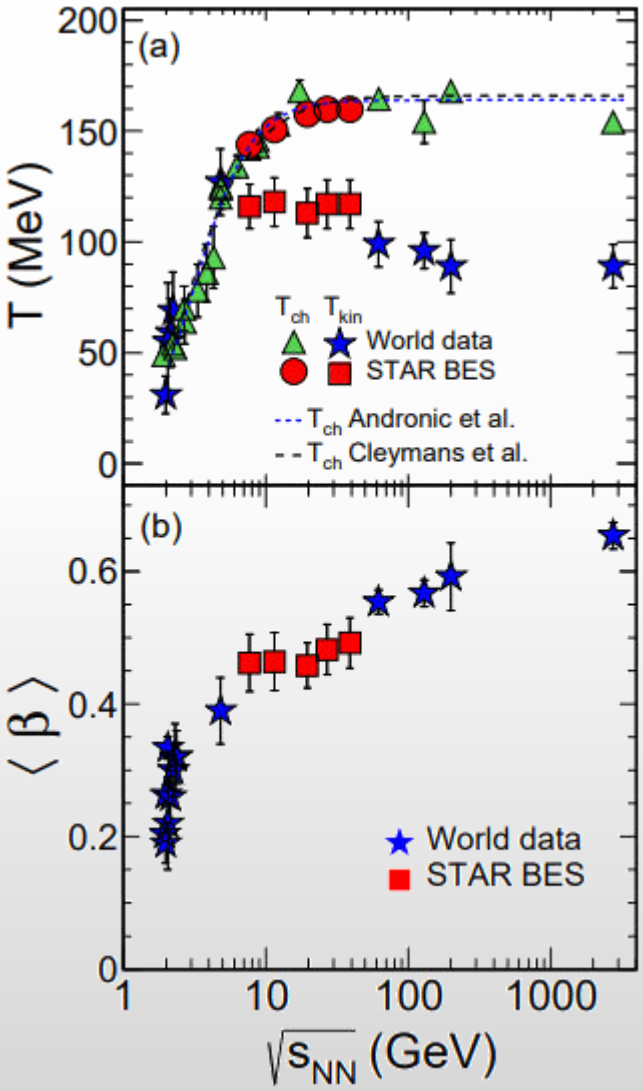

- T_{ch} increases from 7.7 to 19.6 GeV; after that it remains almost constant and similar for all centralities.
- T_{kin} increases from central to peripheral collisions suggesting longer lived fireball in central collisions
- $\langle\beta\rangle$ decreases from central to peripheral collisions suggesting stronger expansion in central collisions.
- The separation between T_{ch} and T_{kin} increases with increasing energy suggesting the effect of increasing hadronic interactions between chemical and kinetic freeze-out at higher energies.

MPD: charged identified light hadrons

- Probe freeze-out conditions, collective expansion, hadronization mechanisms, strangeness production ("horn" for K/π), parton energy loss, etc. with particles of different masses, quark contents/counts
- Charged hadrons: large and uniform acceptance + excellent PID capabilities of TPC and TOF

0-5% central AuAu@9 GeV (PHSD), 5 M events → full event/detector simulation and reconstruction

Phys.Part.Nucl. 53 (2022) 2, 203-206

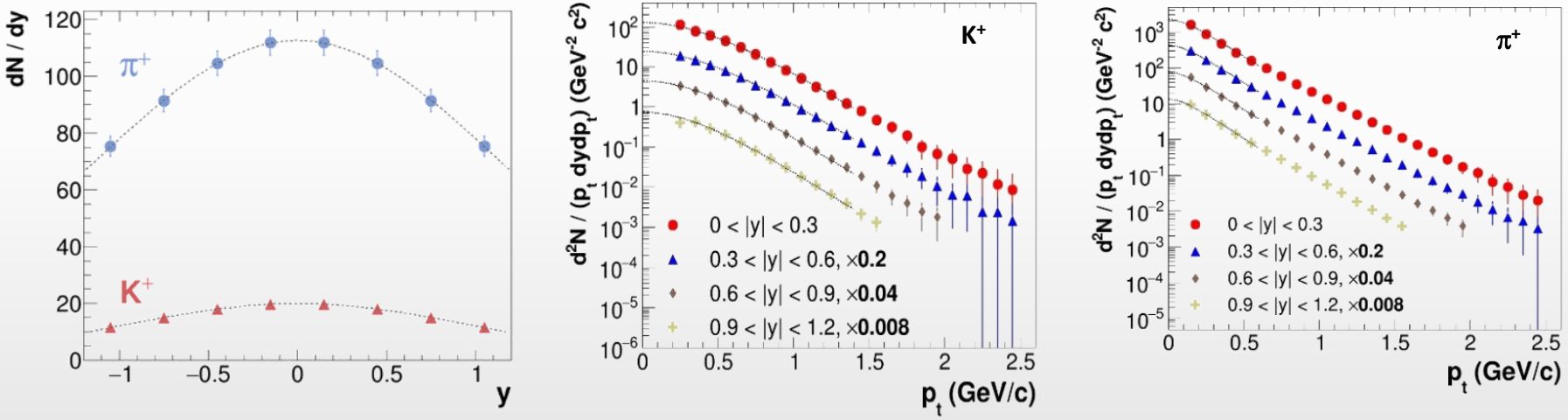

✓ sample ~ 70% of the π/K/p production in the full phase space

✓ hadron spectra are measured from p_T ~ 0.1 GeV/c

MPD: neutral identified light hadrons

- Neutral mesons (π^0, η, K_s, ω, η'): ECAL reconstruction + photon conversion method (PCM)
  - ✓ π^0 ($\pi^0 \to \gamma\gamma$); η ($\eta \to \gamma\gamma$, $\eta \to \pi^0\,\pi^+\,\pi$); K_s ($K_s \to \pi^0\,\pi^0$); ω ($\omega \to \pi^0\,\gamma$, $\omega \to \pi^0\,\pi^+\,\pi$); η' ($\eta' \to \eta\,\pi^+\,\pi$)

AuAu@11 GeV (UrQMD), 10M events → full event/detector simulation and reconstruction

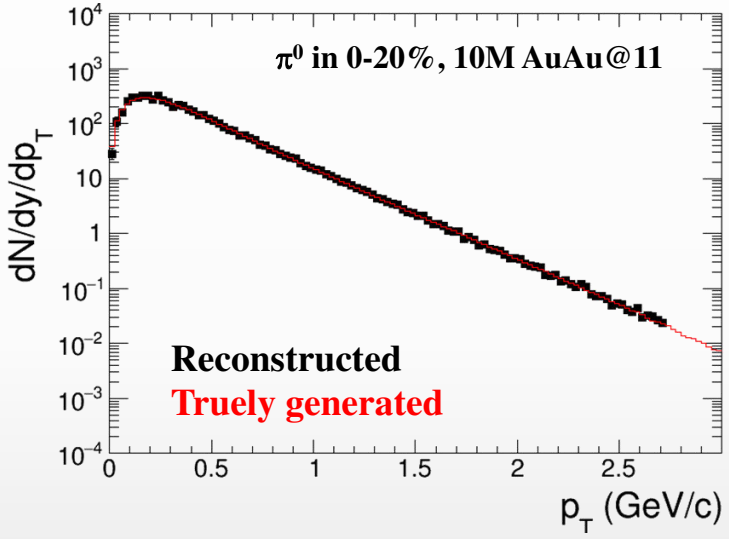

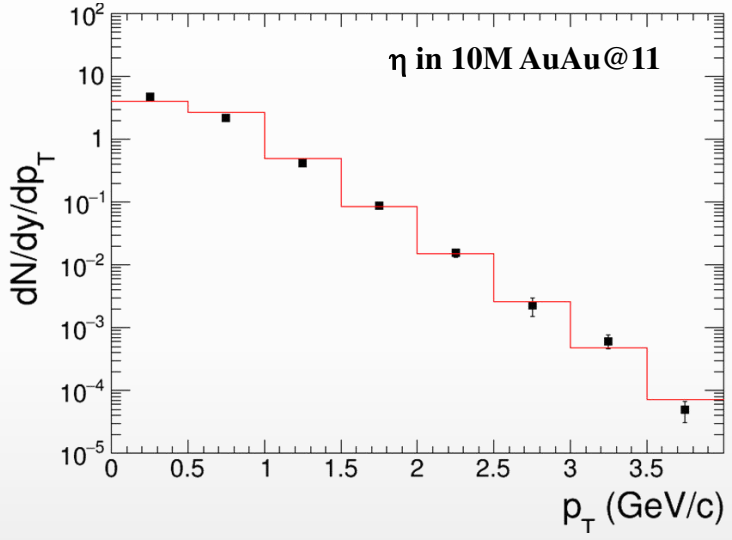

- ✓ extend p_T ranges of charged particle measurements
- ✓ different systematics

MPD will be able to measure differential production spectra, integrated yields and $\langle p_T \rangle$, particle ratios, multiplicity distributions for a wide variety of identified hadrons (π, K, η, ω, p, η')

First measurements will be possible with the first sampled data sets

Hadronic phase

- A phase between chemical and kinetic freeze out → lifetime and conditions?
- Short-lived resonances are sensitive to rescattering and regeneration in the hadronic phase

	ρ(770)	$K^*(892)$	Σ(1385)	Λ(1520)	Ξ(1530)	φ(1020)
cτ (fm/c)	1.3	4.2	5.5	12.7	21.7	46.2
$\sigma_{rescatt}$	$\sigma_\pi\sigma_\pi$	$\sigma_\pi\sigma_K$	$\sigma_\pi\sigma_\Lambda$	$\sigma_K\sigma_p$	$\sigma_\pi\sigma_\Xi$	$\sigma_K\sigma_K$

- Reconstructed resonance yields in heavy ion collisions are defined by:
  - ✓ resonance yields at chemical freeze-out
  - ✓ hadronic processes between chemical and kinetic freeze-outs:

    rescattering: daughter particles undergo elastic scattering or pseudo-elastic scattering through a different resonance → parent particle is not reconstructed → loss of signal

    regeneration: pseudo-elastic scattering of decay products ($\pi K \rightarrow K^{*0}$, $KK \rightarrow \phi$ etc.) → increased yields

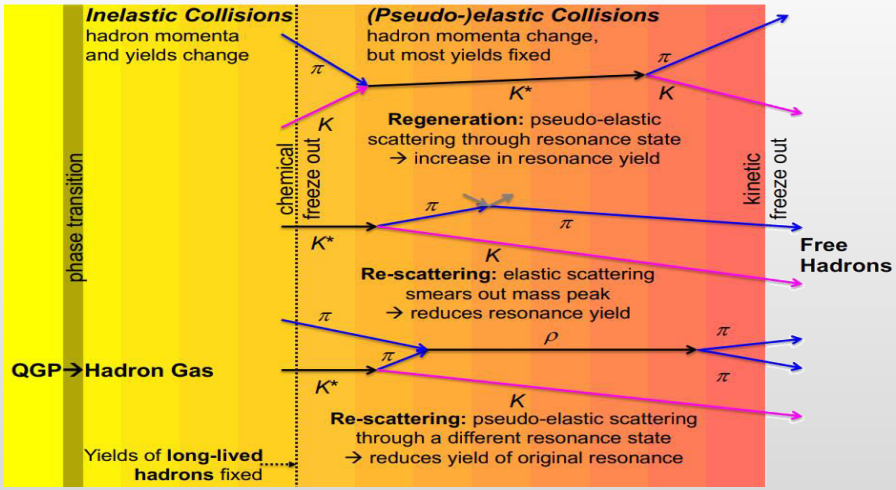

- Resonances provide the means to directly probe the hadronic phase properties

Resonances as probes of the hadronic phase

- Cumulative effect of the hadronic phase effects for resonances depends on:
  - ✓ lifetime and density of the hadronic phase
  - ✓ resonance lifetime and scattering cross sections (type of daughter particles)

- Properties of the hadronic phase are studied by measuring the ratios of the resonance yields (p_T-integrated) to the yields of long-lived particles with similar quark contents: $\rho(770)^0/\pi$, $K^*(892)/K$, $\phi(1020)/K$, $\Lambda(1520)/\Lambda$, $\Sigma(1385)^{\pm}/\Sigma$ and $\Xi(1530)^0/\Xi$

- The ratios are measured as a function of the final state charged-particle multiplicity in pp (reference system), p-A (intermediate) and A+A (heavy-ion) collisions. The variation of the ratios with multiplicity probes the interplay between the rescattering and regeneration effects in the hadronic phase

Experimental results, pp and A+A at the LHC

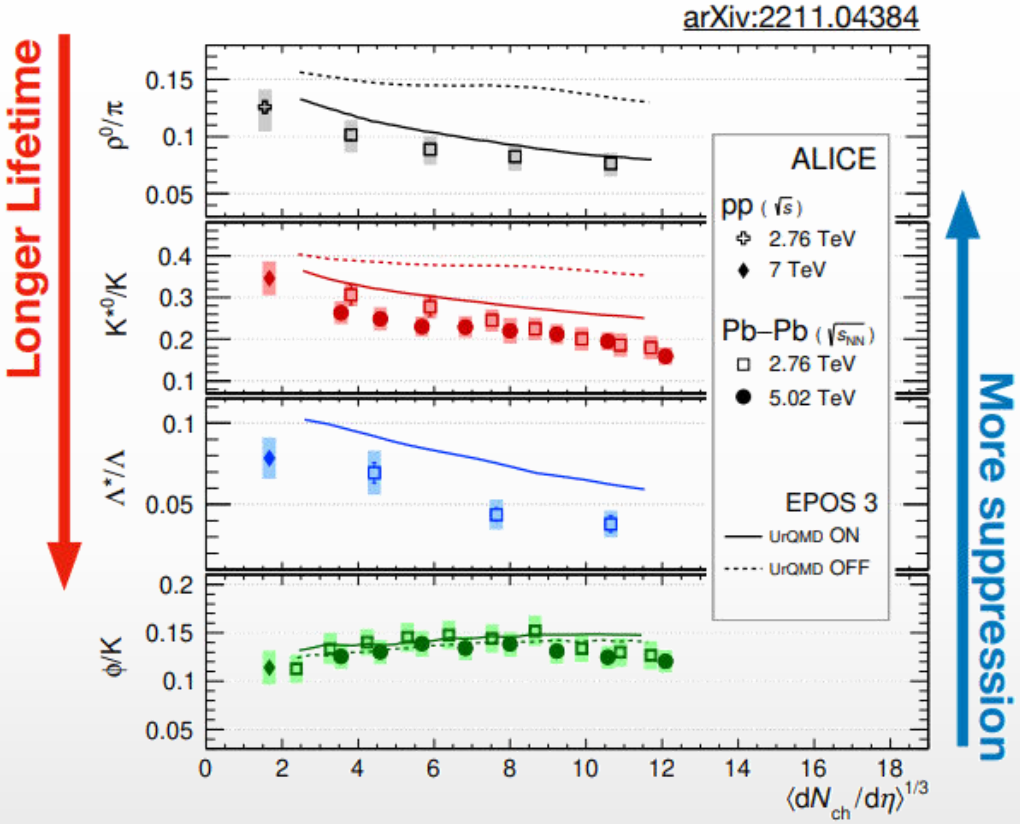

- Suppressed production of short-lived resonances (τ < 20 fm/c) in central A+A collisions → rescattering takes over the regeneration
- No modification is observed for ϕ-meson (τ ~ 40 fm/c) → behaves like a stable particle
- Resonances with intermediate lifetimes show transition from suppression to no effect
- Yield modifications depend on event multiplicity, not on collision system/energy

- Results are qualitatively reproduced by EPOS3 + UrQMD (hadronic phase afterburner)
- Results support the existence of a hadronic phase that lives long enough (τ ~ 10 fm/c) to cause a significant reduction of the reconstructed yields of short-lived resonances
- Hadronic cascade models reproduce the observed suppression
- All model predictions must be filtered through the hadronic phase

MPD: resonance reconstruction

- BiBi@9.2 GeV (UrQMD) after mixed-event background subtraction, 10M events
- Examples of the low-p_T bins

Phys.Scripta 96 (2021) 6, 064002

$\phi(1020) \rightarrow K^+K^-$

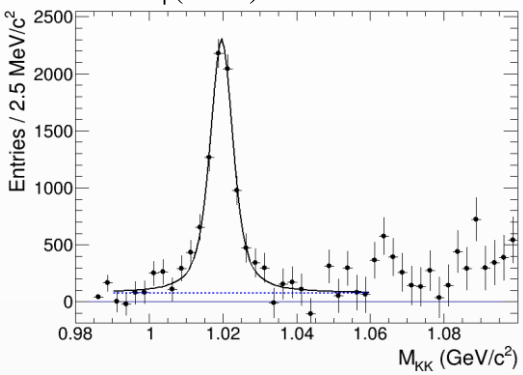

$K^*(892)^0 \rightarrow \pi^\pm K^\pm$

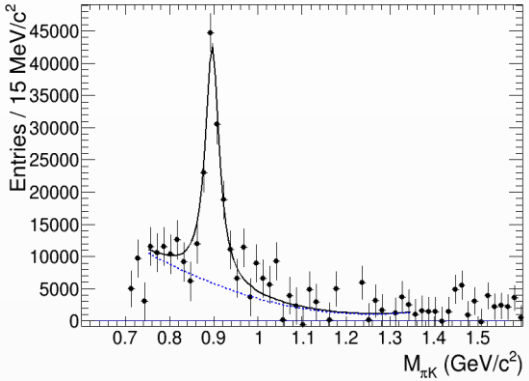

$K^*(892)^\pm \rightarrow \pi^\pm K_s$ ($K_s \rightarrow \pi^+\pi^+$)

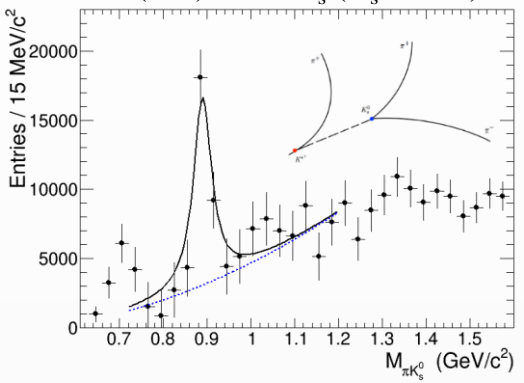

$\Sigma(1385)^\pm \rightarrow \pi^\pm\Lambda$ ($\Lambda \rightarrow p\pi$)

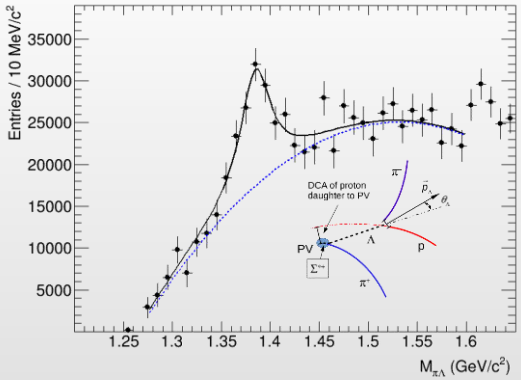

$\Lambda(1520) \rightarrow pK^-$

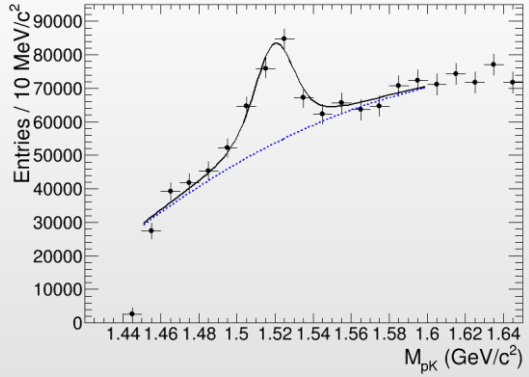

$\Xi(1530)^0 \rightarrow \pi^+\Xi^-$ ($\Xi^- \rightarrow \Lambda\pi^-$, ($\Lambda \rightarrow p\,\pi^-$))

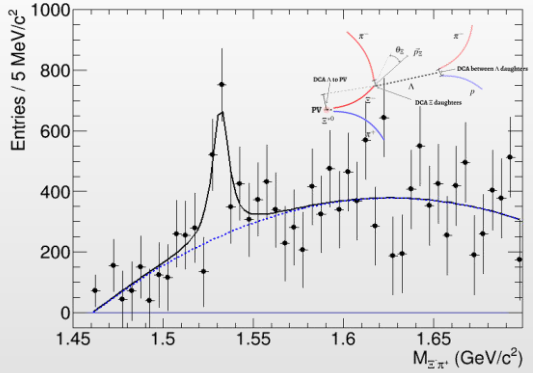

- MPD is capable of resonance reconstruction using: 1) charged hadron identification in the TPC and TOF and 2) measurement of weakly decaying daughters via topological selections
- Measurements are possible starting from ~ <u>zero momentum</u> → sample most of the yields

Direct photons and system temperature

- Direct photons are all photons except for those coming from hadron decays:
  - ✓ produced during all stages of the collision
  - ✓ QGP is transparent for photons → penetrating probe

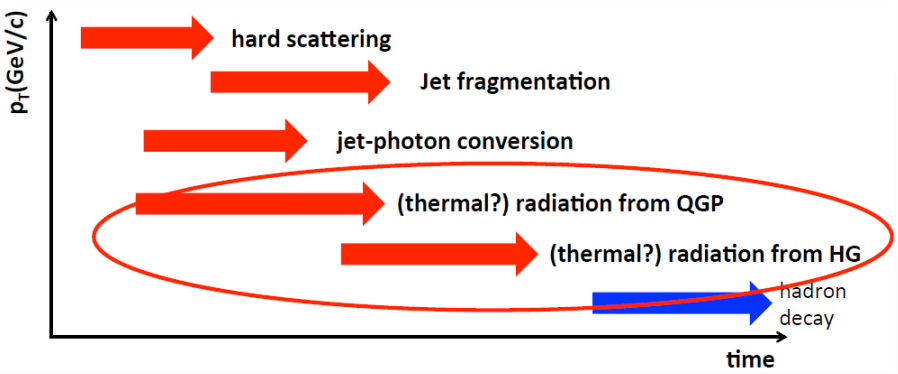

- Low-E photons → effective temperature of the system

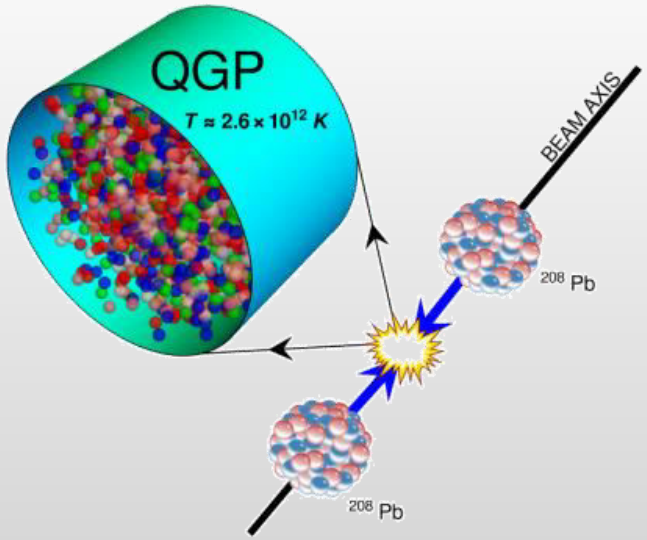

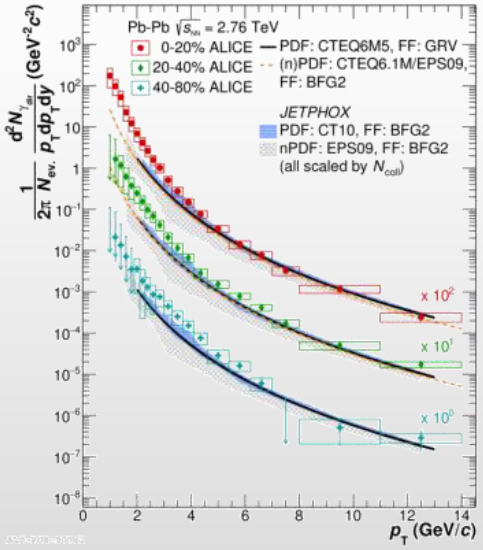

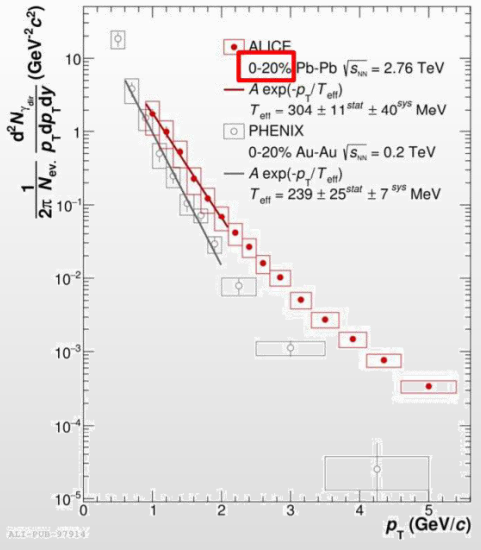

T_{eff} ~ 240 MeV at RHIC; T_{eff} ~ 300 MeV at the LHC

$T_{eff} >> T_c$ ~ 150 MeV predicted by LQCD

Temperature at the center of the Sun ~ 15 000 000 K

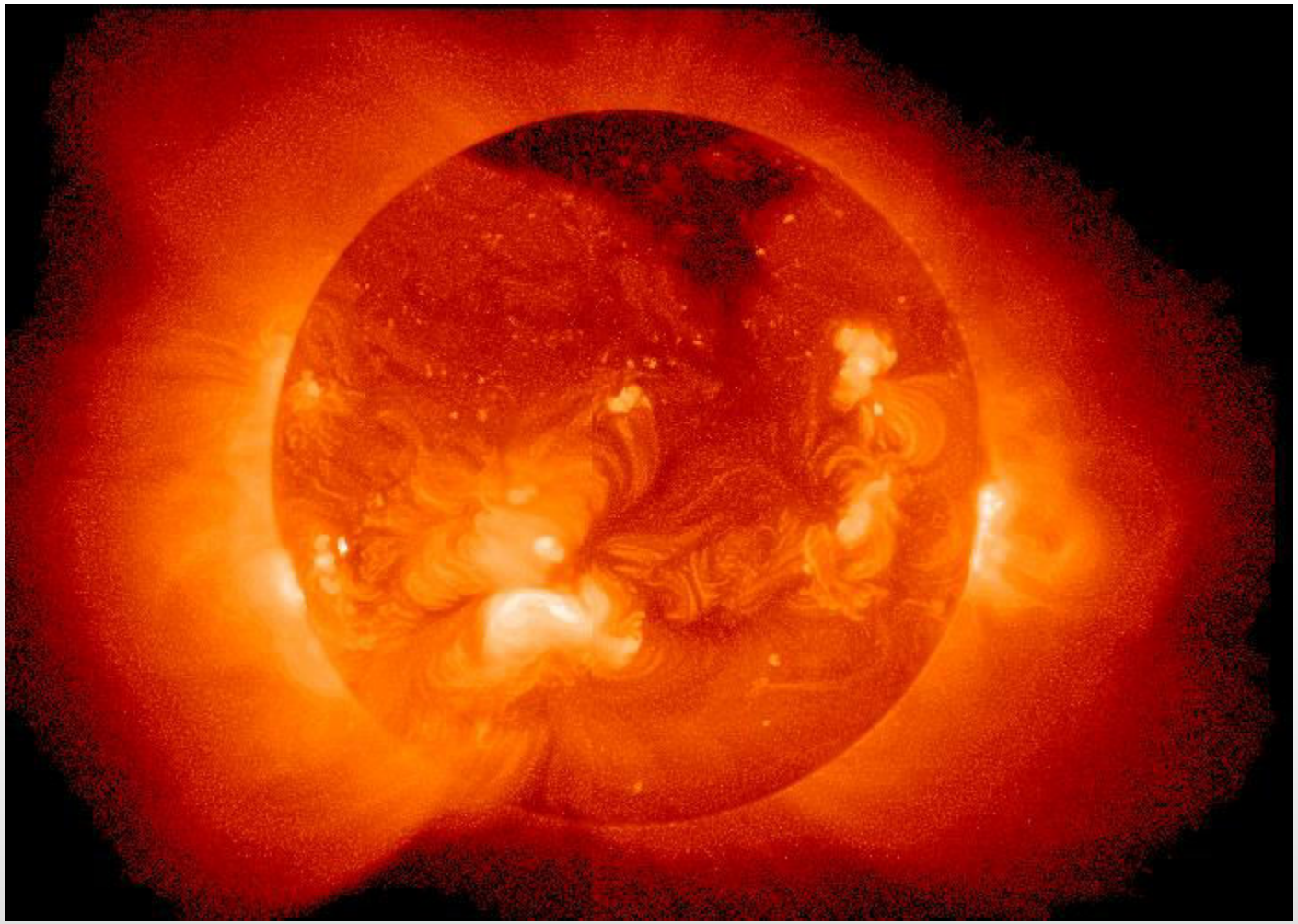

A medium of ~ 200 MeV is more than 100 000 times hotter !!!

MPD: photons

- Photons can be measured in the ECAL or in the tracking system as e^+e^- conversion pairs (PCM)

  beam pipe (0.3% X_0) + inner TPC vessels (2.4% X_0)

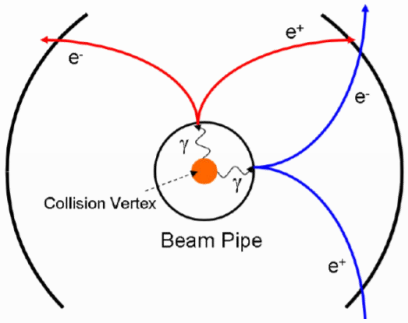

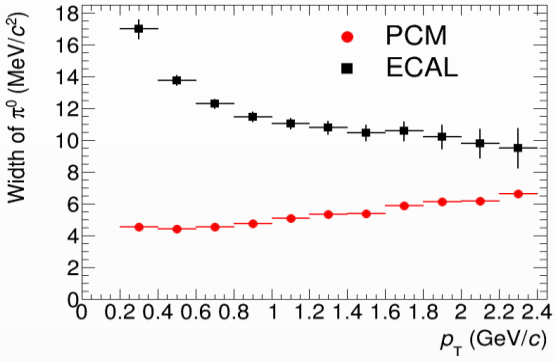

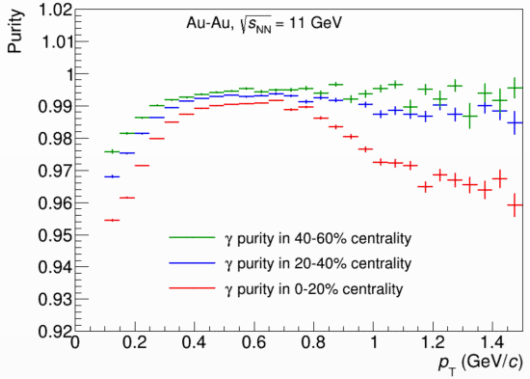

- Main sources of systematic uncertainties for direct photons:
  - ✓ detector material budget → conversion probability
  - ✓ π^0 reconstruction efficiency
  - ✓ p_T-shapes of π^0 and η production spectra

- Use ECAL and PCM for photon reconstruction and measurement of neutral mesons (background)

→ potentially, MPD can provide <u>unique measurements</u> of direct photons in the NICA energy range

Geometry of Heavy-Ion Collisions

Collisions are not all the same

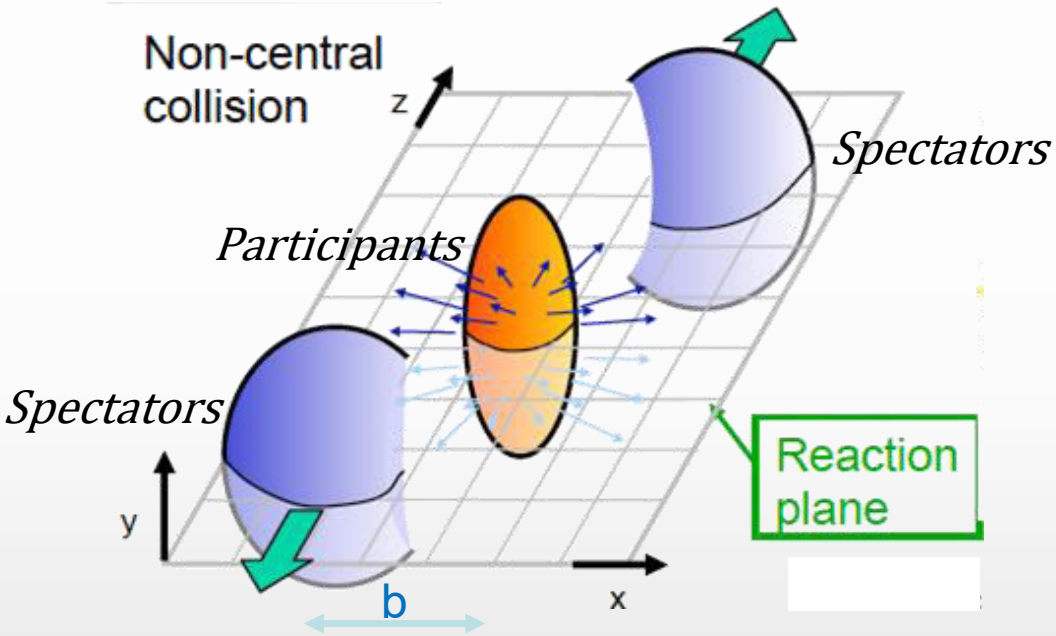

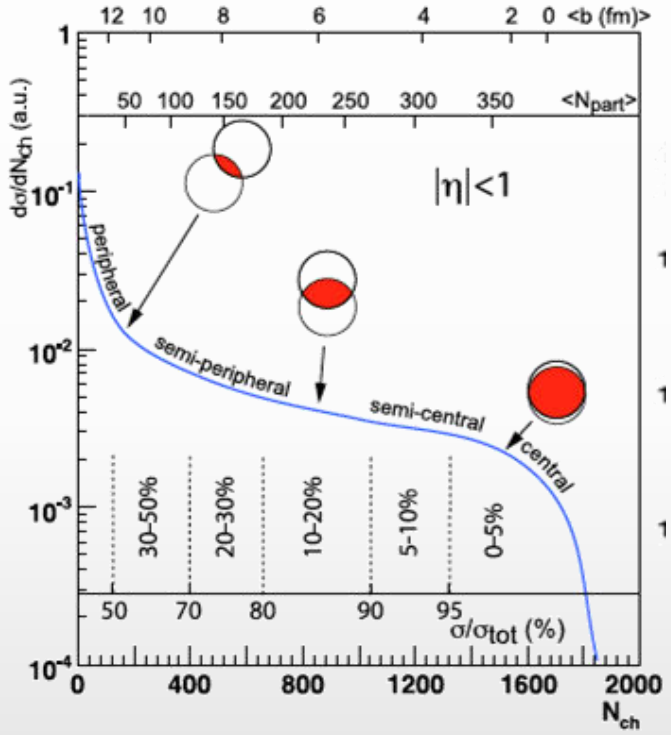

- $N_{participants}$: number of nucleons in the overlap region
- $N_{collisions}$: number of inelastic nucleon-nucleon collisions
- Reaction plane: defined by beam axis and impact parameter
- Centrality: percentile of the total cross section

MC Glauber event

Au+Au at $\sqrt{s_{NN}}$ = 200 GeV b = 6 fm

Transverse plane

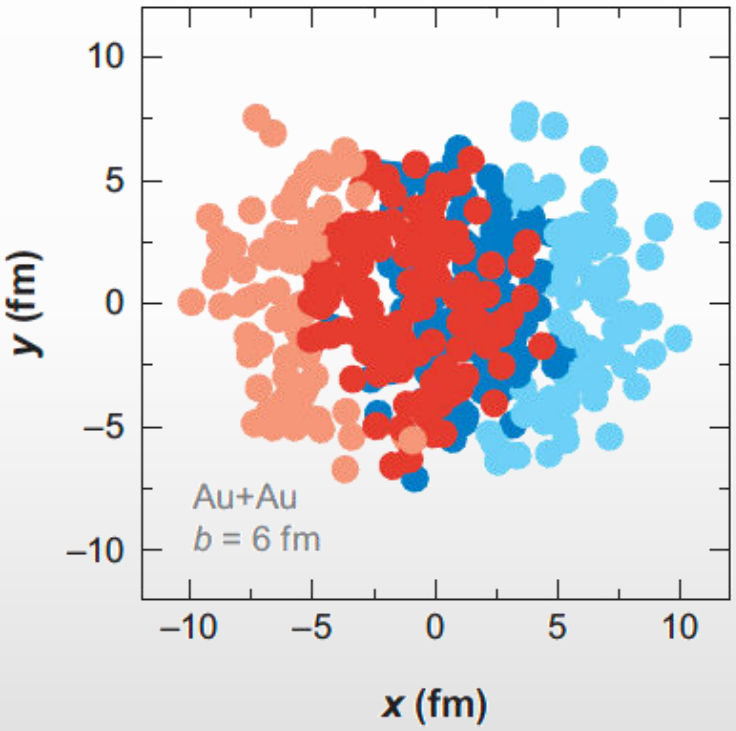

Along the beam axis

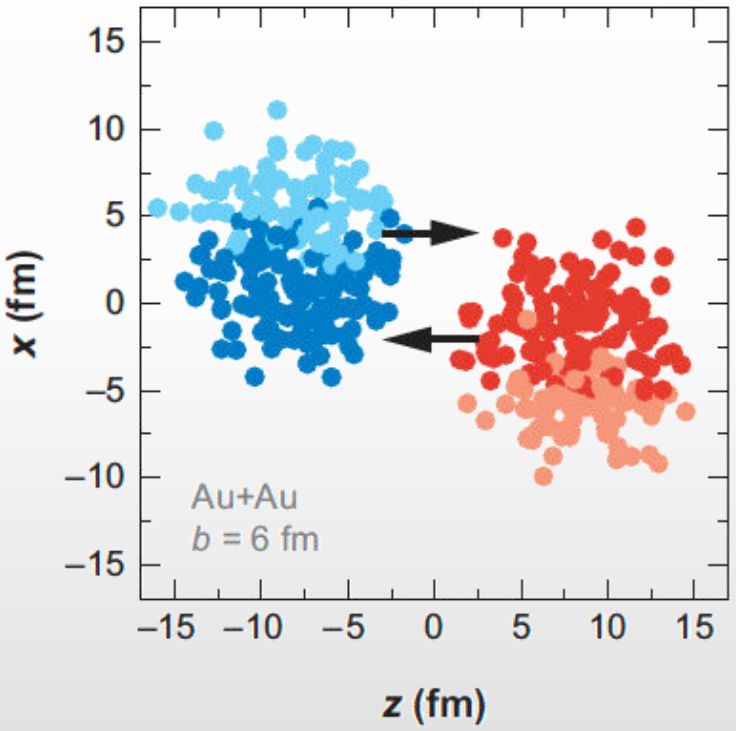

The nucleons are drawn with radius $\sqrt{\sigma_{\text{inel}}^{\text{NN}}/\pi}/2$

Darker circles represent participating nucleons

$\langle N_{part} \rangle$ and $\langle N_{coll} \rangle$

$\sqrt{s_{NN}}$= 200 GeV Au+Au collision
Inelastic NN cross section σ_{NN} = 42 mb
a = 0.53 fm R_{Au} = 6.38 fm

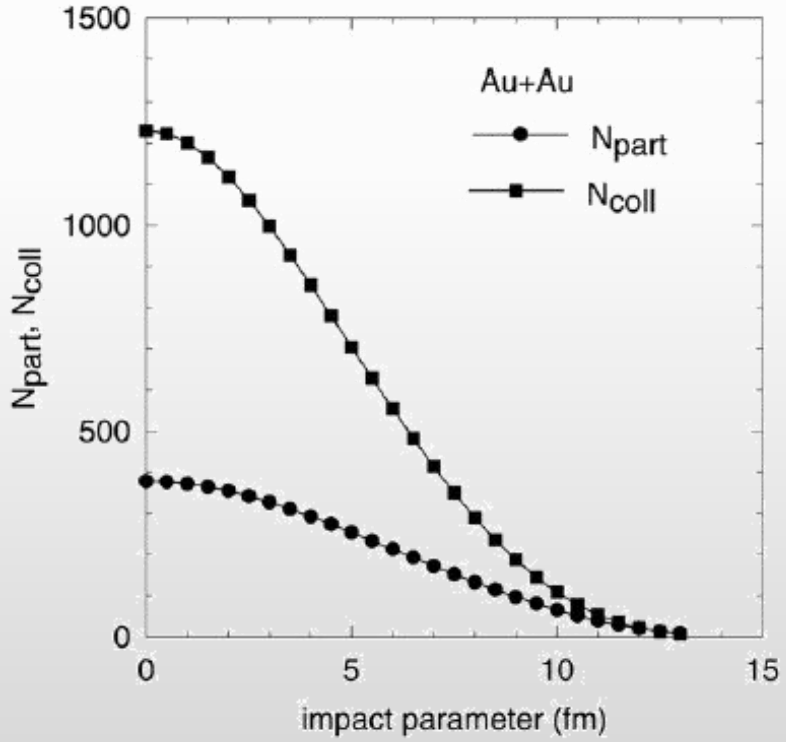

Azimuthal anisotropy of particles in HIC

S. Voloshin, Y. Zhang, Z. Phys. C70,(1996), 665

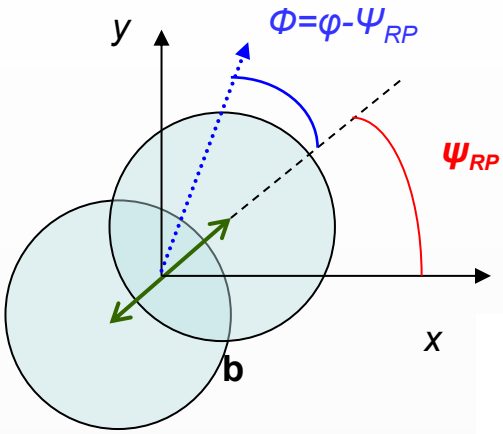

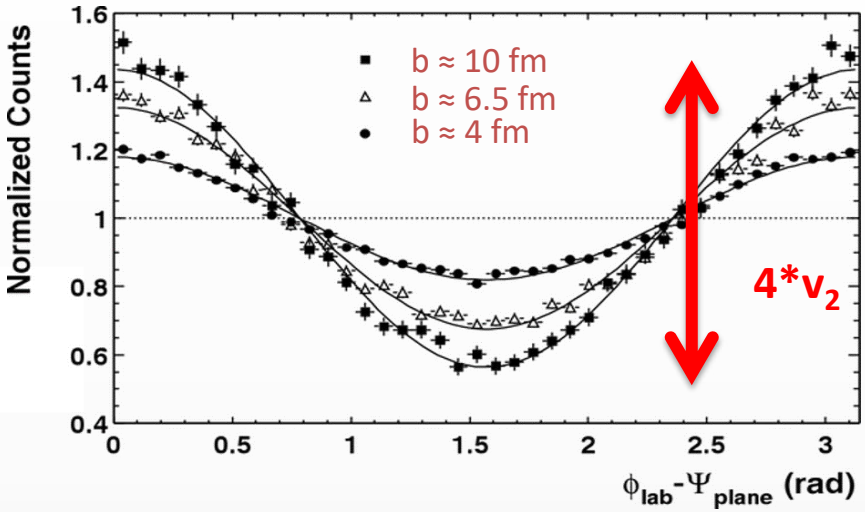

$$\frac{dN}{d(\varphi-\Psi_{RP})}=\frac{N_0}{2\pi}\left(1+2v_1\cos(\varphi-\Psi_{RP})+2v_2\cos(2(\varphi-\Psi_{RP}))+....\right)$$

- The sinus terms are skipped by symmetry arguments
- From the properties of Fourier's series one has

$$v_n=\langle\cos[n(\varphi-\Psi_{RP})]\rangle$$

- Fourier coefficients V_n quantify anisotropic flow:

v_1 is directed flow, v_2 is elliptic flow, v_3 is triangular flow, etc.

Term "flow" is used only to emphasize the collective behavior of particles

Anisotropic flow at RHIC/LHC

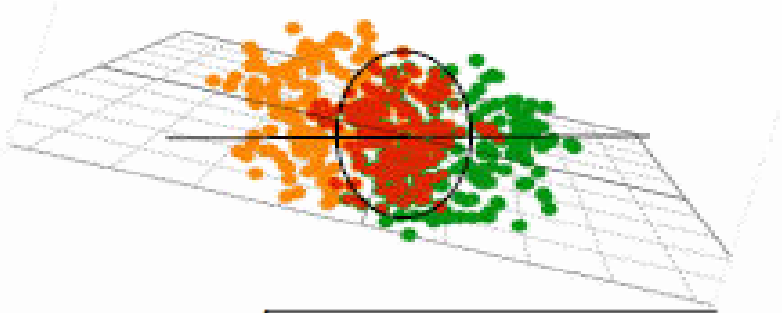

$$\epsilon_n = \sqrt{\frac{\langle r^n \cos n\phi \rangle + \langle r^n \sin n\phi \rangle}{\langle r^n \rangle}}$$

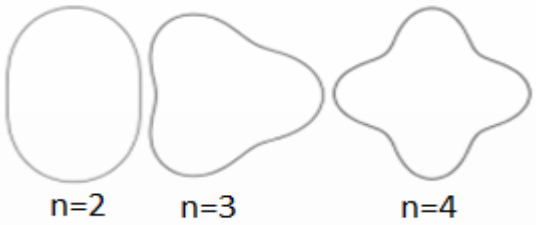

$$\frac{dN}{d\phi} \propto \left(1 + 2\sum_{n=1} v_n \cos\left[n\left(\phi - \Psi_n\right)\right]\right)$$

❖ Initial eccentricity and its fluctuations drive momentum anisotropy v_n with specific viscous modulation

Gale, Jeon et al., Phys. Rev. Lett. 110, 012302

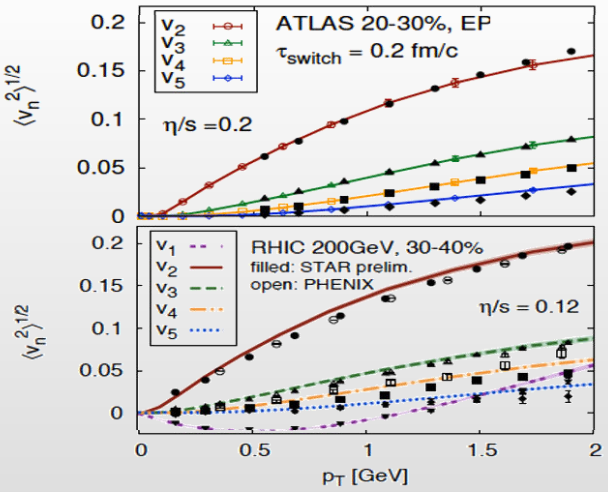

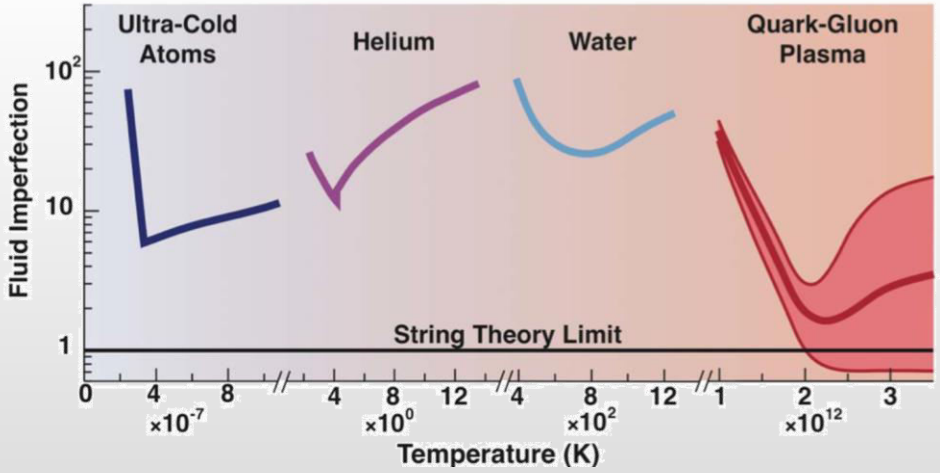

❖ Evidence for a dense <u>perfect liquid</u> found at RHIC/LHC (M. Roirdan et al., Scientific American, 2006)

Beam energy dependence

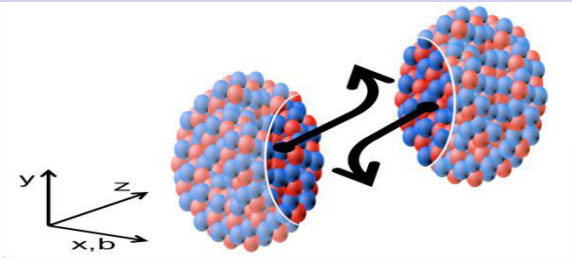

- Generated during the nuclear passage time $(2R/\gamma)$ – sensitive to EOS
- RHIC @ 200 GeV $(2R/\gamma) \sim 0.1$ fm/c
- AGS @ 3-4.5 GeV $(2R/\gamma) \sim 9$-5 fm/c
- v_1 and v_2 show strong centrality, energy and species dependence

Phys.Rev.Lett. 112 (2014) 16, 162301

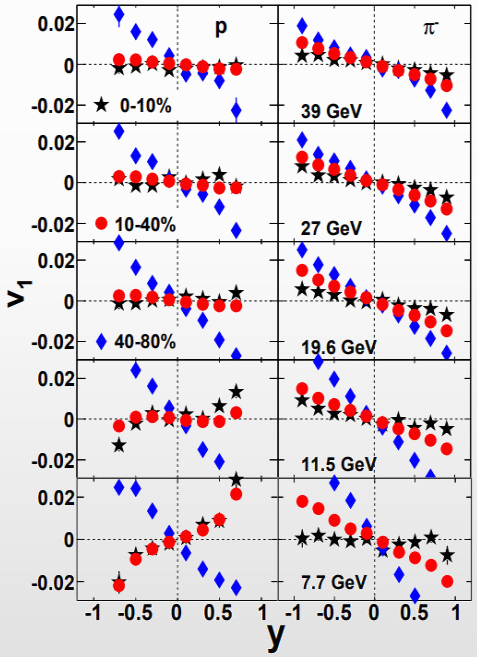

EPJ Web Conf. 204 (2019) 03009

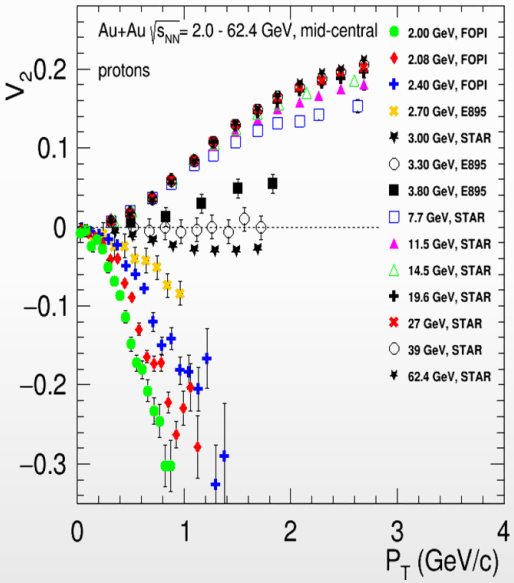

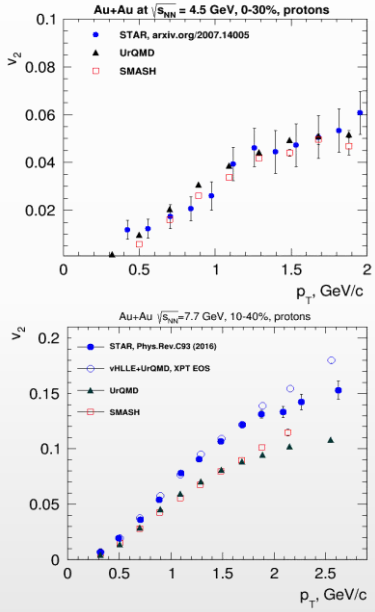

- ✓ $\sqrt{s_{NN}} \sim$ 3-4.5 GeV, pure hadronic models reproduce v_2 (JAM, UrQMD) → degrees of freedom are the interacting baryons
- ✓ $\sqrt{s_{NN}} \geq 7.7$ GeV, need hybrid models with QGP phase (vHLLE+UrQMD, AMPT with string melting,…)

At NICA energies, flow is highly sensitive to fireball expansion and interactions with spectators
Flow is a probe of the dominant degrees of freedom (hadronic vs. partonic)

MPD: v_2 for π/p, v_3 for h±

AuAu@7.7 GeV (UrQMD), 15 M events → full event/detector simulation and reconstruction

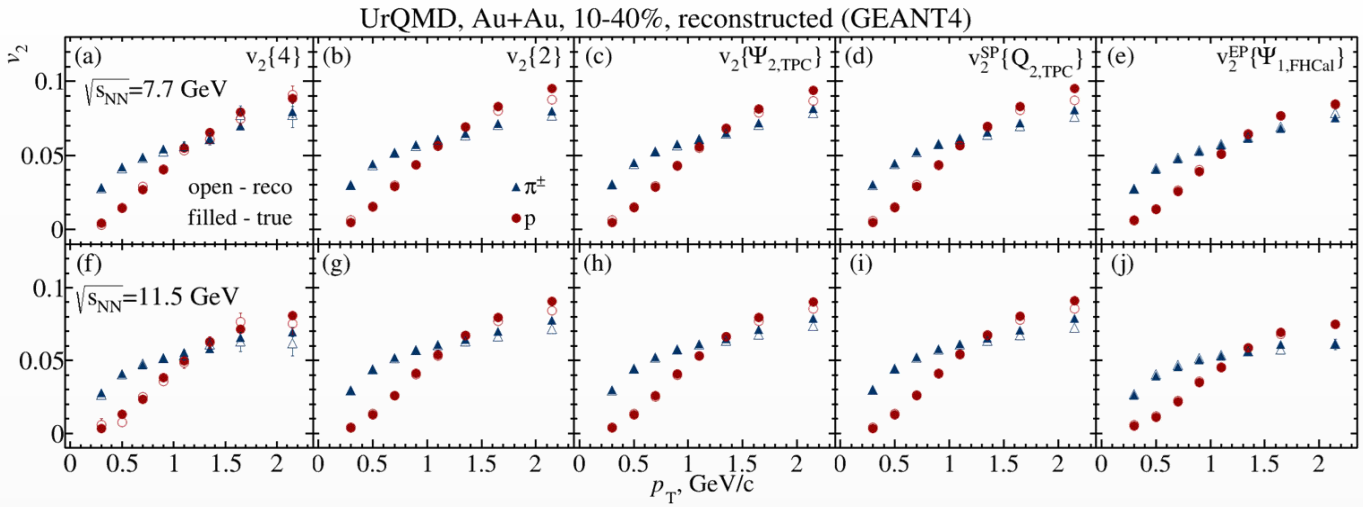

AuAu@11.5 GeV (vHLLE + UrQMD), 15 M events → full event/detector simulation and

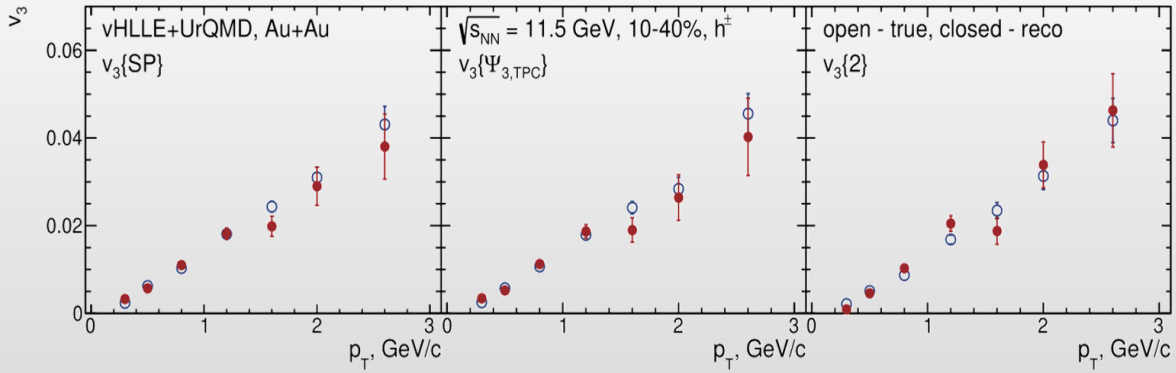

- Reconstructed and generated v_2 of pions and protons and v_3 of charged hadrons are in good agreement
- Models show that higher harmonic ripples are more sensitive to the existence of a QGP phase

MPD: v_1, v_2 for V0 (K^0_s and Λ)

AuAu@11 GeV (UrQMD), 25 M events → full event/detector simulation and reconstruction

$$v_2^{SB}(m_{inv},p_T) = v_2^{S}(p_T)\frac{N^{S}(m_{inv},p_T)}{N^{SB}(m_{inv},p_T)} + v_2^{B}(m_{inv},p_T)\frac{N^{B}(m_{inv},p_T)}{N^{SB}(m_{inv},p_T)}$$

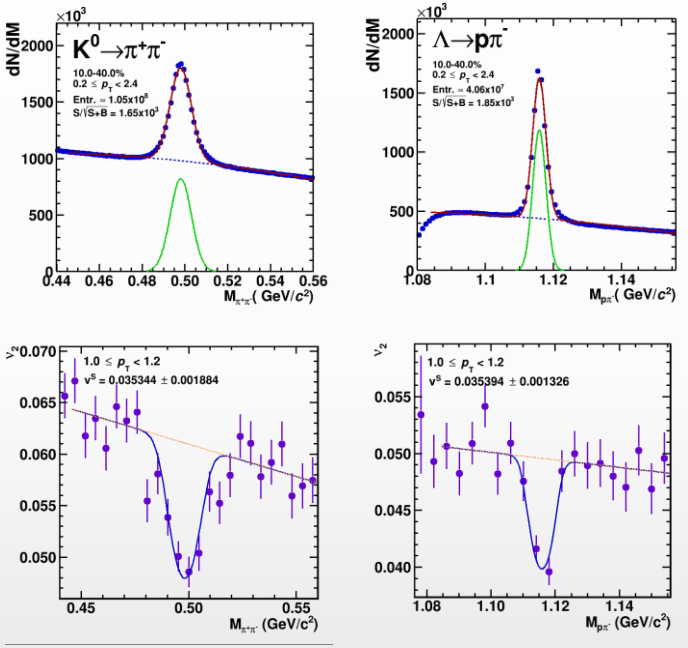

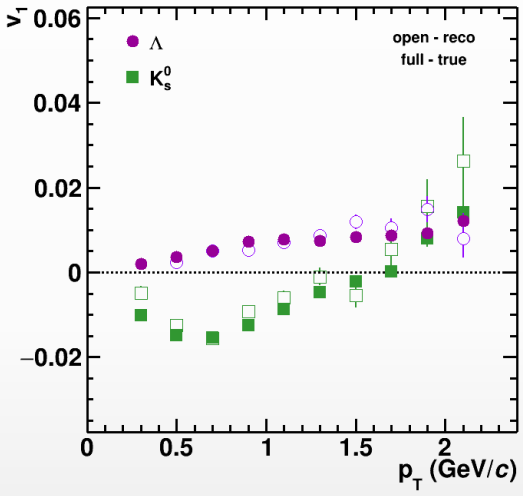

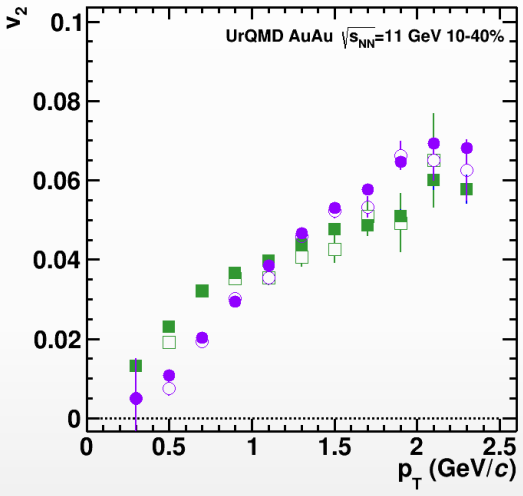

- Differential flow signal extraction using invariant mass fit method
- Reasonable agreement between reconstructed and generated v_n signals for K^0_s and Λ

MPD has capabilities to measure different flow harmonics for a wide variety of identified hadrons
→ constraints for model approaches, dominant degrees of freedom

System size scan (p-A and A-A) for flow measurements is a unique capability of the MPD in the NICA energy range

Conclusions

- Столкновения тяжелых (ультра)релятивистских ядер позволяет изучать свойства сильновзаимодействующей (КХД) материи в условиях экстремальных температур и (нет)барионных плотностей
- Исследование подобных состояний требует измерения импульсных, энергетических и угловых распределений для рождающихся частиц (фотоны, адроны, лептоны) в широком динамическом диапазоне (p_T, быстрота)
- Интерпретация полученных результатов требует тесной кооперации с содружеством теоретиков
- Эксперименты на коллайдере NICA позволят изучить область фазовой диаграммы, соответствующей сравнительно небольшим температурам, но максимальным (нет)барионных плотностям.
- Программа физических исследований на коллайдере NICA предлагает ряд уникальных возможностей

BACKUP

Charged particle tracker – Drift Chamber

- A long evolution of gaseous tracking detectors: Geiger-Muller counter → Proportional counter → (Multiwire) proportional chamber → Drift chamber (DC) and Time Projection Chamber (TPC)
- Drift chamber of the PHENIX experiment at RHIC:

Wire potentials: Uc = -4.5 kV, Ug = -1.6 kV, Ub = -2 kV, Us - grounded
Wire diameters: B, G, C ~ 100 μm, S ~ 25 μm

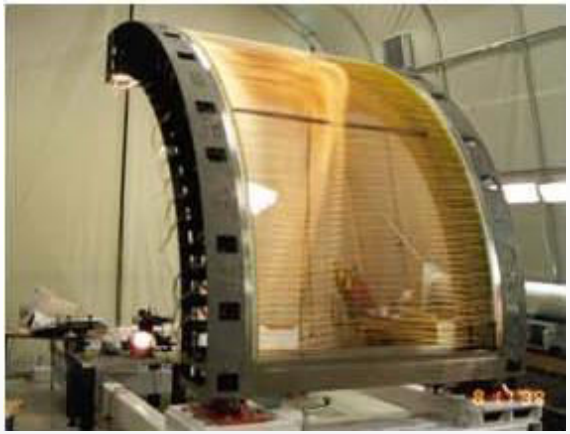

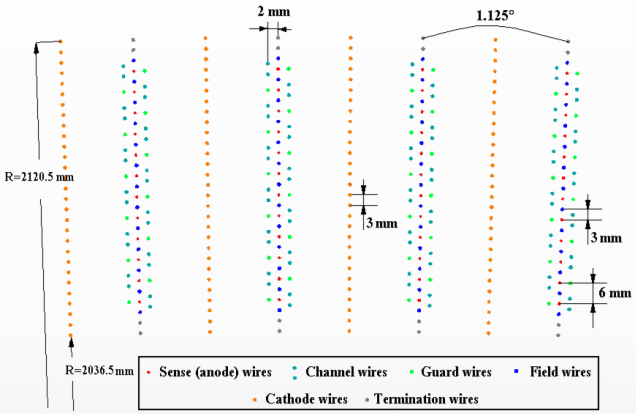

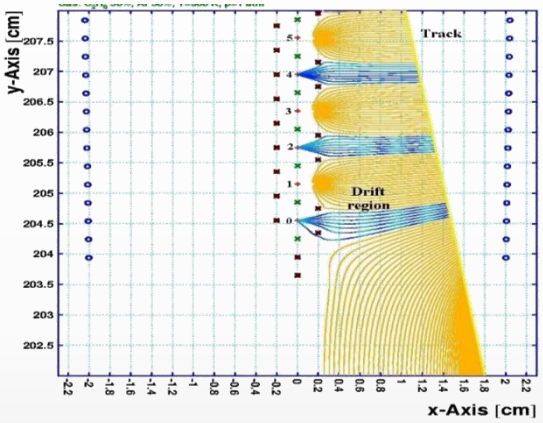

- ✓ Large gas volume of a few m^3 filled with specific gas mixtures to provide constant v_e and high GA: Ar-C_2H_6, 50%-50%
- ✓ Wires of different types and thickness have different voltages applied to produce required electric field configuration
- ✓ Charged particle produces electron-ion pairs along the path in the had mixture (Ar-C_2H_6, 50%-50%)
- ✓ Electrons drift towards the plane of sensitive (S) wires, v_e ~ 50 μm/ns → 2 cm drift in ~ 400 ns
- ✓ Drifting electrons are amplified next to S-wires in strong electric field (E ~ q/r)
- ✓ Measurable signal is detected on S-wires → drift time from the ionization region, T_d
- ✓ Drift time is converted to the drift distance, L = v_e * T_d → one point in space (efficiency ~100%, resolution ~120μm)
- ✓ 10-20 points are measured along the path → track reconstruction → magnetic field analysis → $\delta p/p = \sqrt{(0.5\%)^2+(1\%\cdot p)^2}$
- ✓ Double-track resolution ~ 1 cm

Further developments: Micro-Pattern Gas Detectors

- Position-sensitive detectors based on wire structures are limited by basic diffusion processes and space charge effects to localization accuracies of ~100 μm
- MPGD are developed to provide high rate capability (up to 10^6 Hz/mm^2) and excellent spatial resolution (down to 30 μm), large sensitive area and dynamic range and superior radiation hardness
- A broad family of MPGD technologies are being developed and optimized: Micro-Strip Gas Chamber (MSGC), Gas Electron Multiplier (GEM), Micro-Mesh Gaseous Structure (Micromegas), THick GEMs (THGEM), Resistive Plate WELL (RPWELL), GEM-derived architecture (μ-RWELL), Micro-Pixel Gas Chamber (μ-PIC), etc.

GEM (Gas Electron Multiplier)

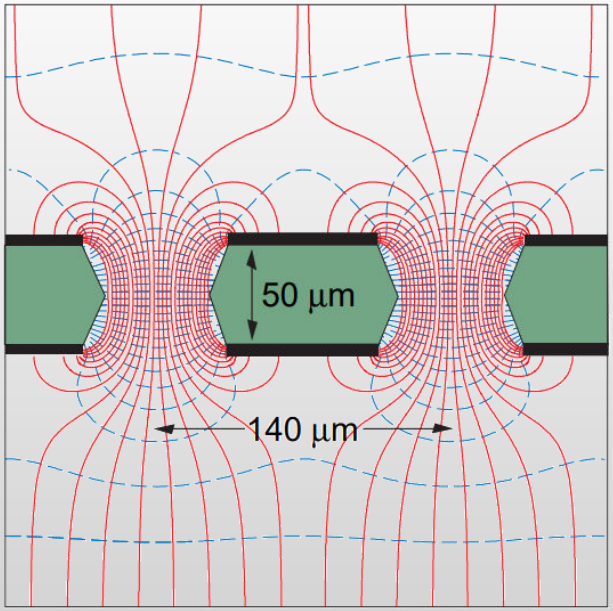

microMEGAS

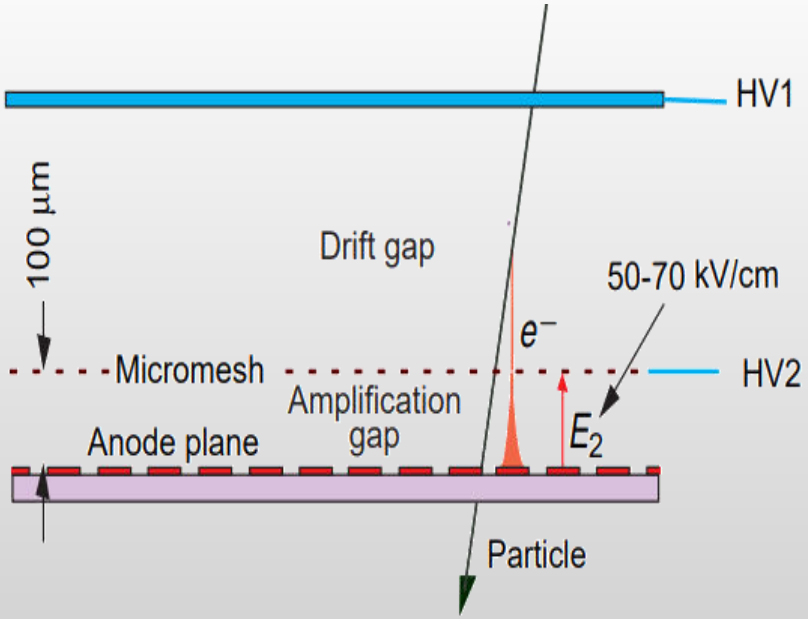

Cherenkov detectors

- Used as a threshold detector for electron identification and/or hadron identification at high momenta
- Cherenkov light is emitted along the particle trajectory if it moves faster than c/n, n – refraction index

$$\cos(\theta_c) = \frac{1}{n\beta}$$

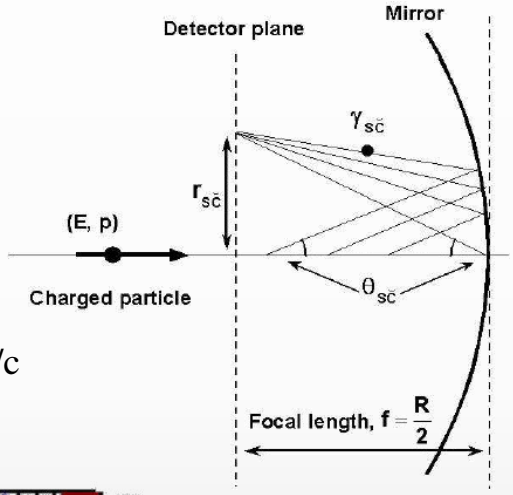

- ✓ Threshold detector, v > c/n
- ✓ Light emitted at constant angle θ_c along the particle path make a circle on the read-out plane → Ring Imaging Cherenkov Detector (RICH)
- ✓ Particle velocity β defines circle radius → separation up to tens of GeV/c

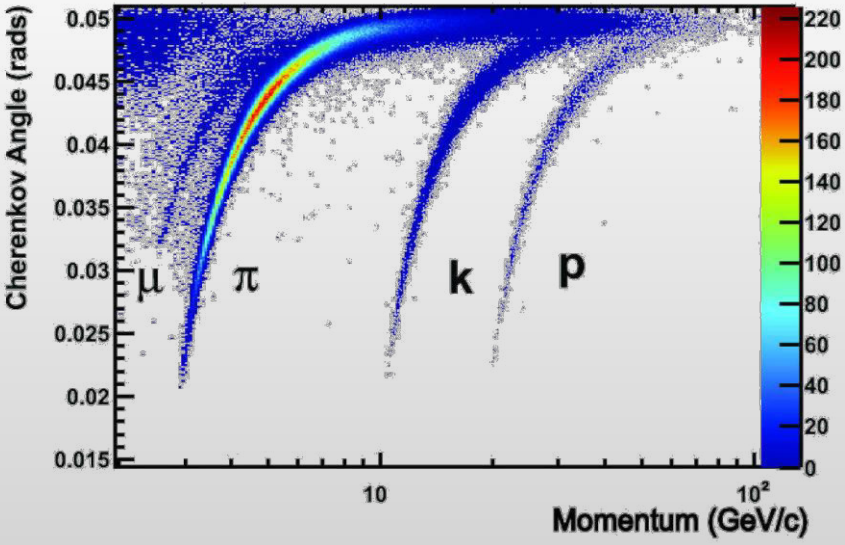

Electron identification

- Electrons are produced at low rates, $e/\pi \sim 10^{-3}$-10^{-4}
- Identification of electrons requires special treatment using capabilities of different detectors

TPC: log(dE/dx)

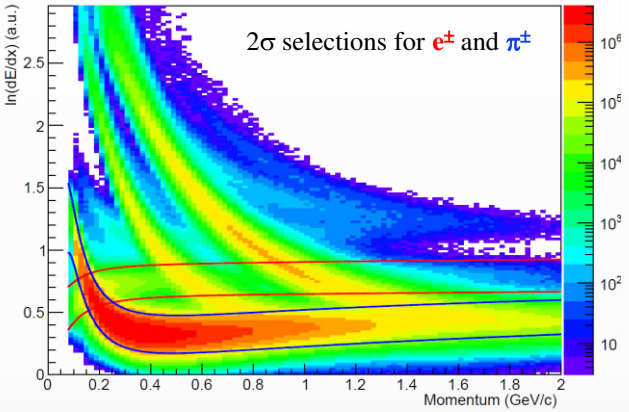

- ✓ eID at low momentum
- ✓ $e^{\pm}$ and $\pi^{\pm}$ bands merge at ~ 200 MeV/c

TOF: β ~ 1, p_T > 150 MeV/c

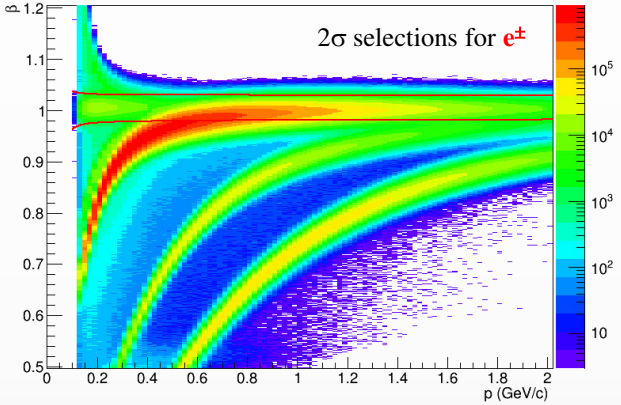

- ✓ $e^{\pm}$ with p_T < 150 MeV/c miss the TOF
- ✓ $e^{\pm}$ and $\pi^{\pm}$ bands merge at ~ 400 MeV/c

ECAL: tof < 2 ns (δ ~ 500 ps) + E/p ~ 1

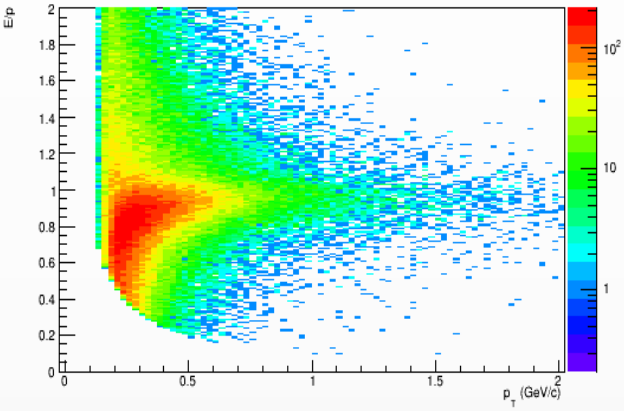

- ✓ $e^{\pm}$ with p_T < 200 MeV/c miss the ECAL
- ✓ E/p ~ 1 for $e^{\pm}$ at p_T > 300-400 MeV/c

- Each of the detectors provides more efficient electron identification in a limited range of momenta
- Combined use of the TPC-TOF-ECAL signals enhances the probability for a selected track to be true $e^{\pm}$

Electron identification

- Electrons are produced at low rates, $e/\pi \sim 10^{-3}$-10^{-4}
- Identification of electrons requires special treatment using capabilities of different detectors

TPC: log(dE/dx)

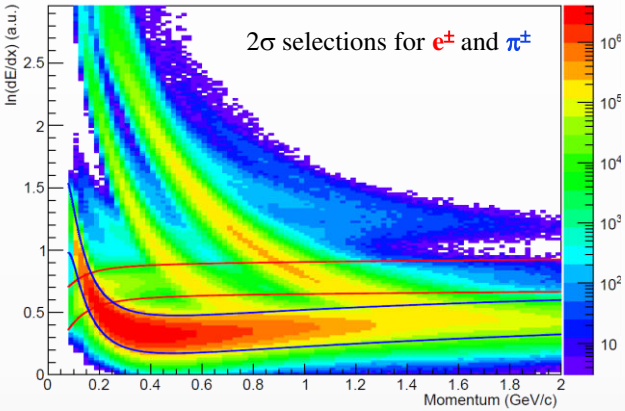

- ✓ eID at low momentum
- ✓ $e^{\pm}$ and $\pi^{\pm}$ bands merge at ~ 200 MeV/c

TOF: β ~ 1, p_T > 150 MeV/c

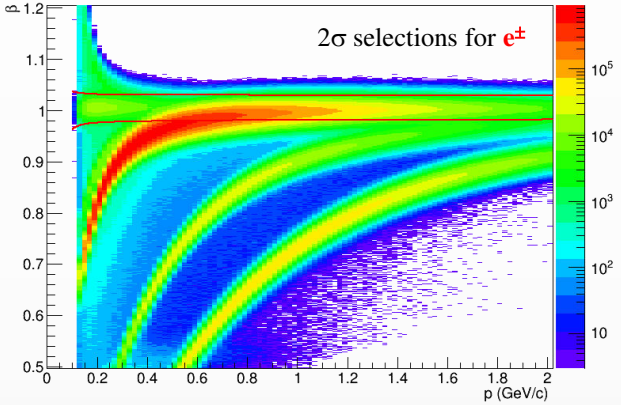

- ✓ $e^{\pm}$ with p_T < 150 MeV/c miss the TOF
- ✓ $e^{\pm}$ and $\pi^{\pm}$ bands merge at ~ 400 MeV/c

ECAL: tof < 2 ns (δ ~ 500 ps) + E/p ~ 1

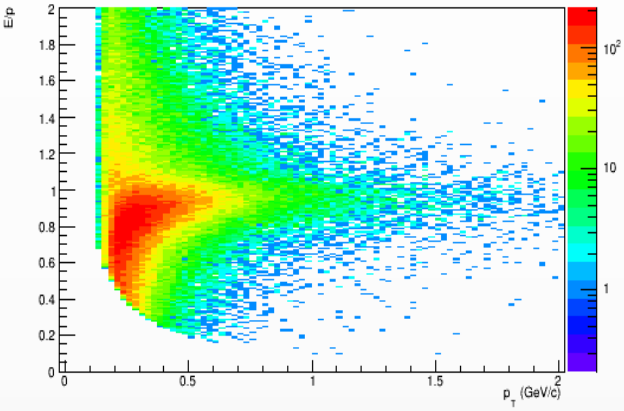

- ✓ $e^{\pm}$ with p_T < 200 MeV/c miss the ECAL
- ✓ E/p ~ 1 for $e^{\pm}$ at p_T > 300-400 MeV/c

- Each of the detectors provides more efficient electron identification in a limited range of momenta
- Combined use of the TPC-TOF-ECAL signals enhances the probability for a selected track to be true $e^{\pm}$

Electron efficiency and purity

- Simulated BiBi@9.2 GeV, realistic vertex distribution
- Selected tracks:
  - ✓ hits > 39
  - ✓ |η| < 1
  - ✓ |DCA_x,y,z| < 3 σ
  - ✓ 2σ matching to TOF
  - ✓ 1-2σ TPC-eID
  - ✓ 2σ TOF-eID

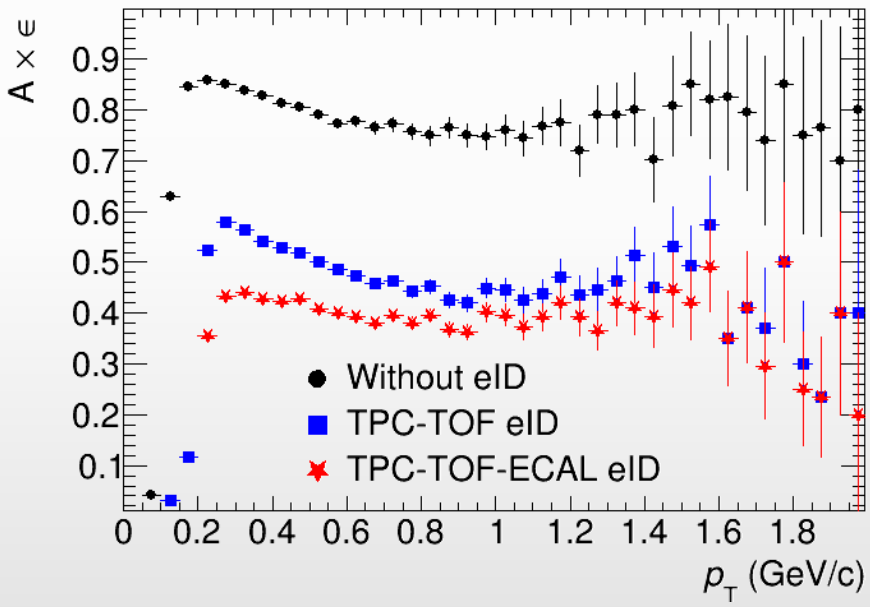

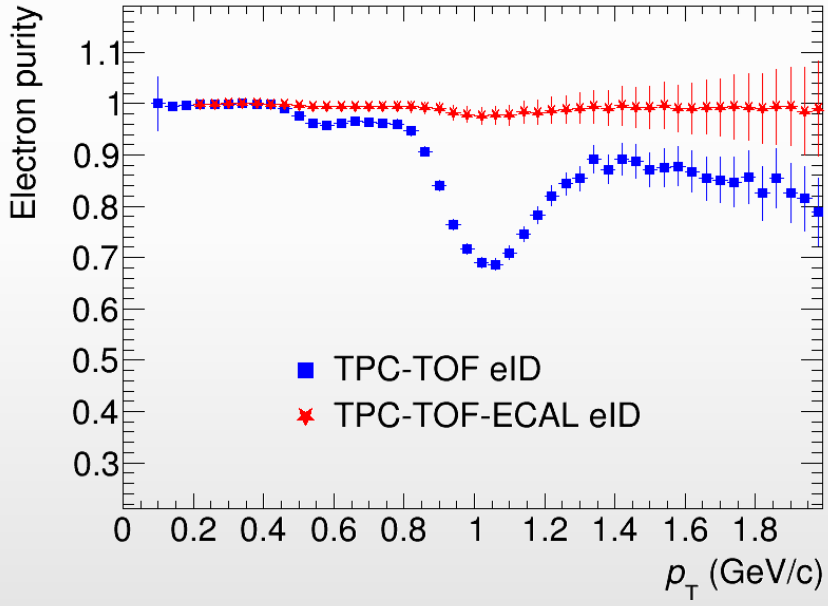

- Purity of ~ 100% at 40% reconstruction efficiency can be achieved at p_T > 150 MeV/c

Hadronic phase lifetime

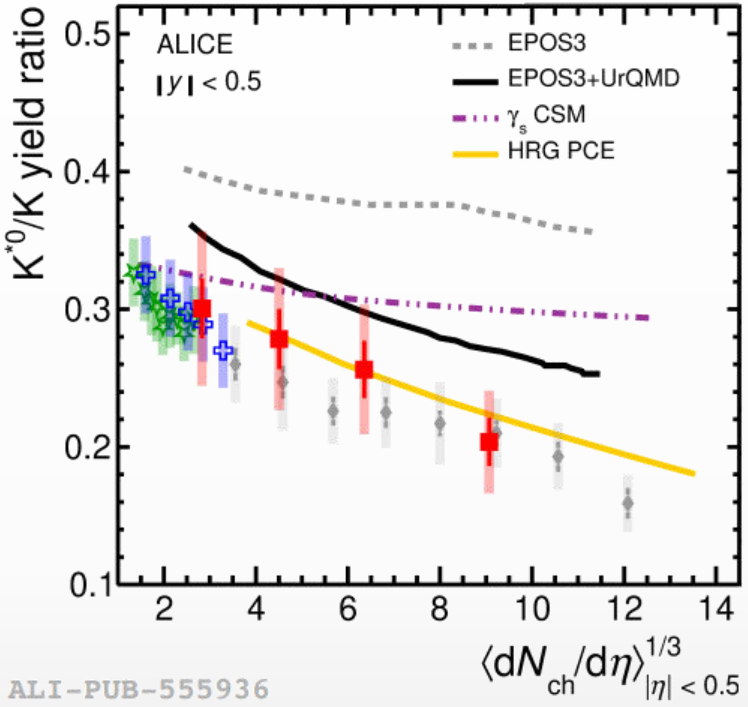

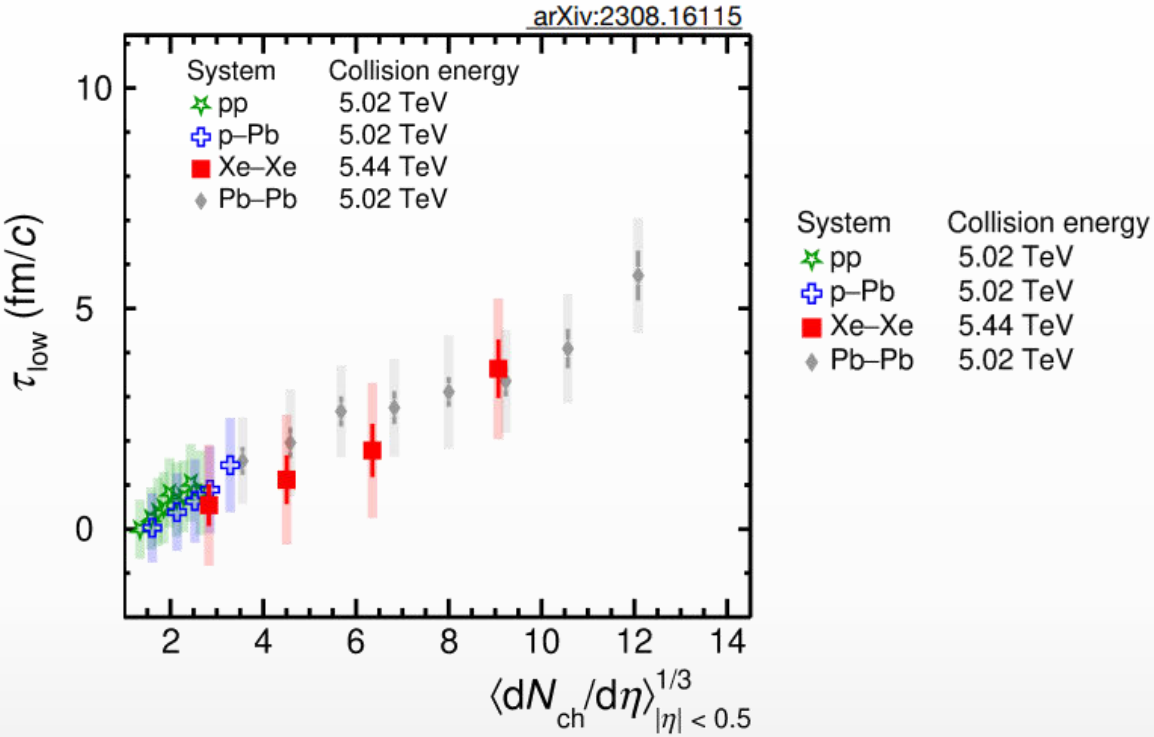

$$r_{\mathrm{kin}} = r_{\mathrm{chem}} \times e^{-(\tau_{\mathrm{kin}}-\tau_{\mathrm{chem}})/\tau_{\mathrm{res}}}$$

- **Lower bound on the hadronic phase lifetime**
  - r_{kin}: Particle ratio at kinetic freeze-out (Pb-Pb)
  - r_{chem}: Particle ratio at chemical freeze-out (pp)
  - τ_{res}: lifetime of resonance
  - **Assumptions:**
    Simultaneous freeze-out of all particles
    Negligible regeneration
  - Scaled with Lorentz factor $\sqrt{1+(\frac{<p_T>}{\text{mass of } K^{*0}})^2}$

- ❖ Lower limit for hadronic phase lifetime ~ 7 fm/*c* in central A-A
- ❖ Smooth evolution of hadronic phase lifetime with multiplicity
- ❖ Hadronic cascade models reproduce the observed suppression
- ❖ All model predictions must be filtered through the hadronic phase

Reconstruction of hypertritons

BiBi@9.2 GeV (PHQMD), 40 M events → full event/detector simulation and reconstruction

Phys.Part.Nucl.Lett. 19 (2022) 1, 46-53

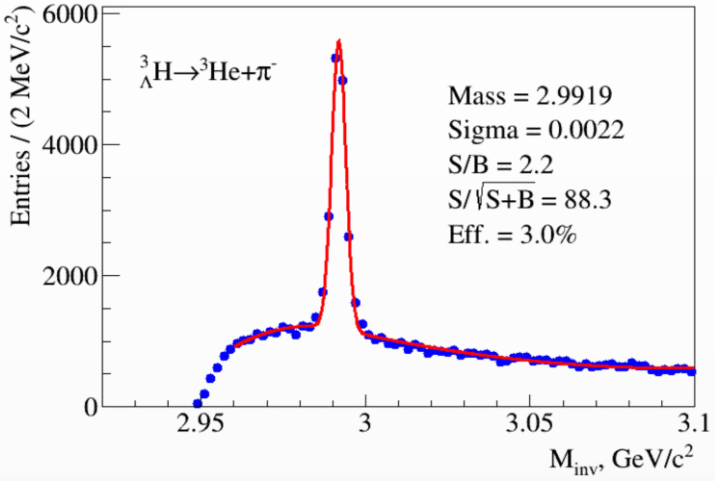

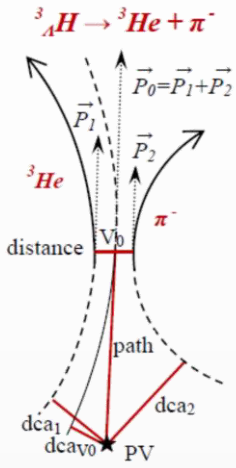

Decay channel	Branching ratio	Decay channel	Branching ratio
$\pi^- + {}^3He$	**24.7%**	$\pi^- + p + p + n$	1.5%
$\pi^0 + {}^3H$	12.4%	$\pi^0 + n + n + p$	0.8%
$\pi^- + p + d$	**36.7%**	$d + n$	0.2%
$\pi^0 + n + d$	18.4%	$p + n + n$	1.5%

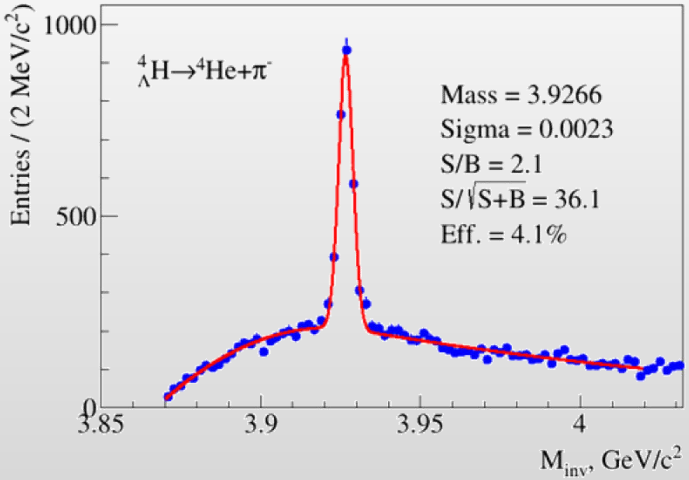

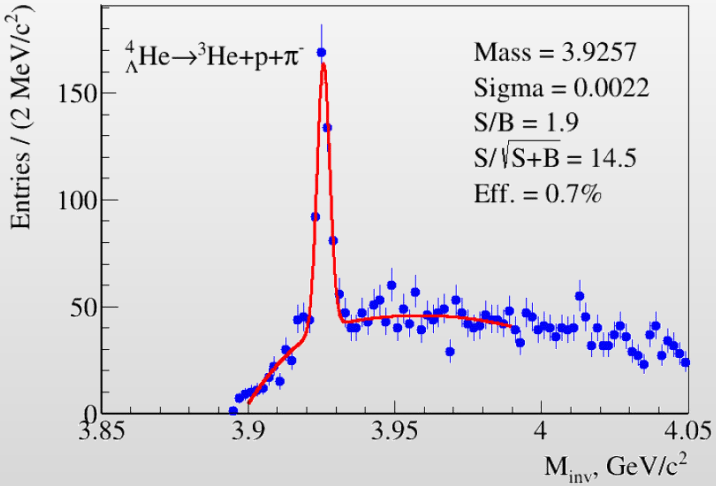

Nuclear modification factor, R_{AA}

- Jet-quenching effect is expected in QGP:
  - ✓ hard scattered parton traverses the dense and hot medium (QGP) created in HIC
  - ✓ parton interacts with the medium (radiative and multiple scattering losses) and then fragments to colorless hadrons
  - ✓ due to energy loss in the medium, the mean momentum of hadrons produced in fragmentation is lower
  - ✓ energy loss ~ medium properties → jet quenching is studied to infer properties of the medium → QGP

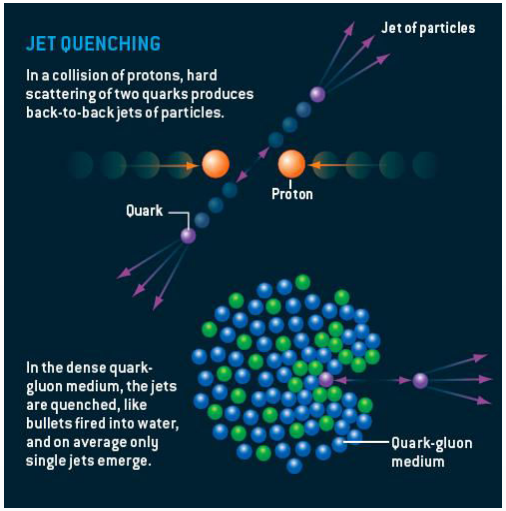

- In practice, jet quenching can be studied by measuring nuclear modification factors for high-p_T hadrons produced in parton fragmentation

- Nuclear modification factor:

$$R_{AA} = \frac{dN_{AA}/dy}{\langle N_{coll} \rangle \cdot dN_{pp}/dy}$$

Rare processes like hard scattering scale with N_{coll}

Hard scattering dominated particle production at $p_T >$ 3-5 GeV/c

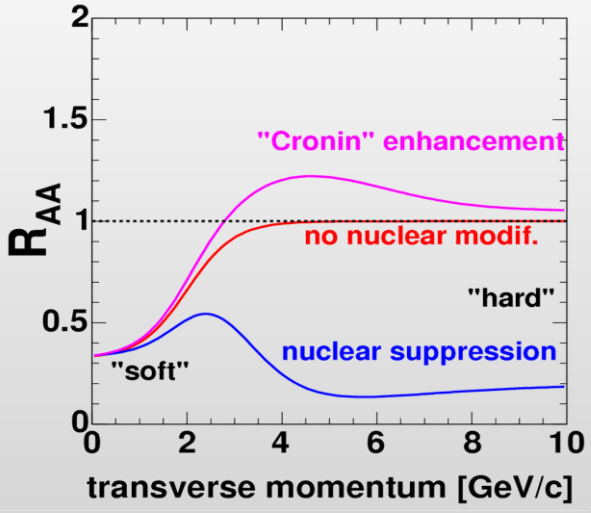

R_{AA} for high-p_T direct photons

- Prompt direct photons are produced in hard scattering processes (very early in the collision)
- Produced medium (QGP) is transparent for photons → R_{AA} should be ~ 1 ???

PHENIX, PRL 94, 232301

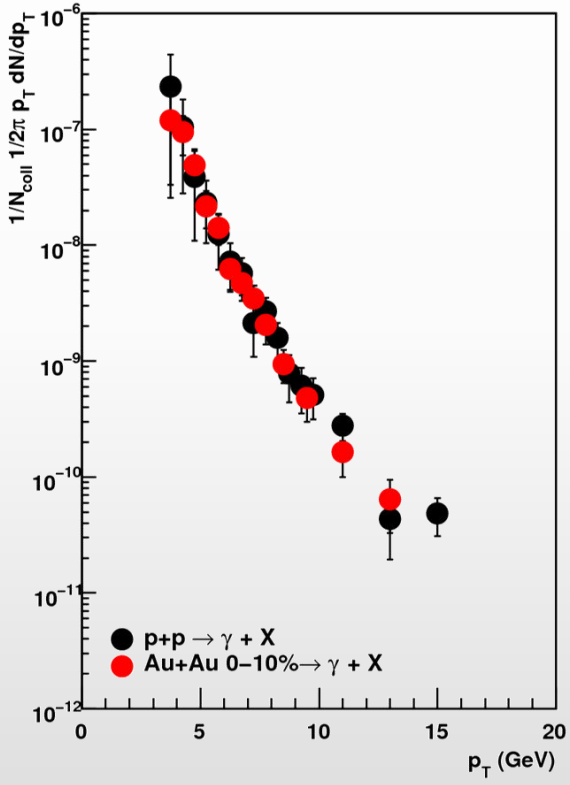

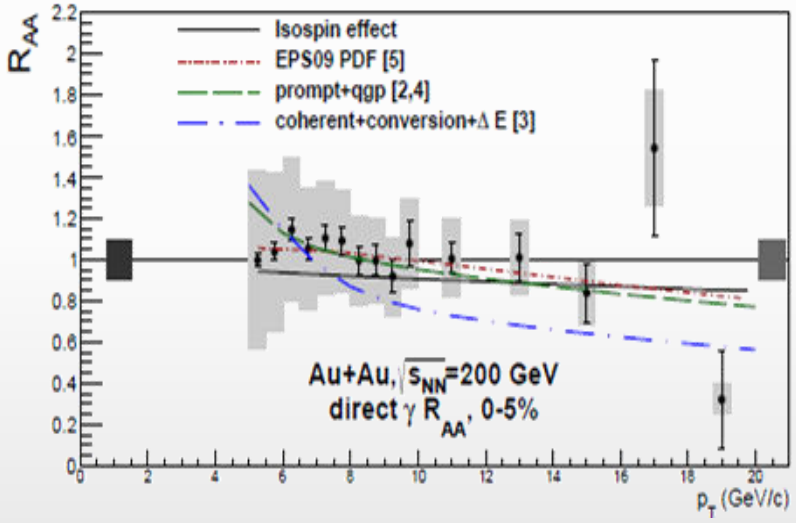

Indeed, R_{AA} ~ 1 → verification for Glauber model used to estimate N_{coll}

R_{AA} for high-p_T hadrons

❖ If partons loose energy while traversing the medium (QGP) → R_{AA} should be < 1 ???

Phys.Rev.C87 (2013) 3, 034911

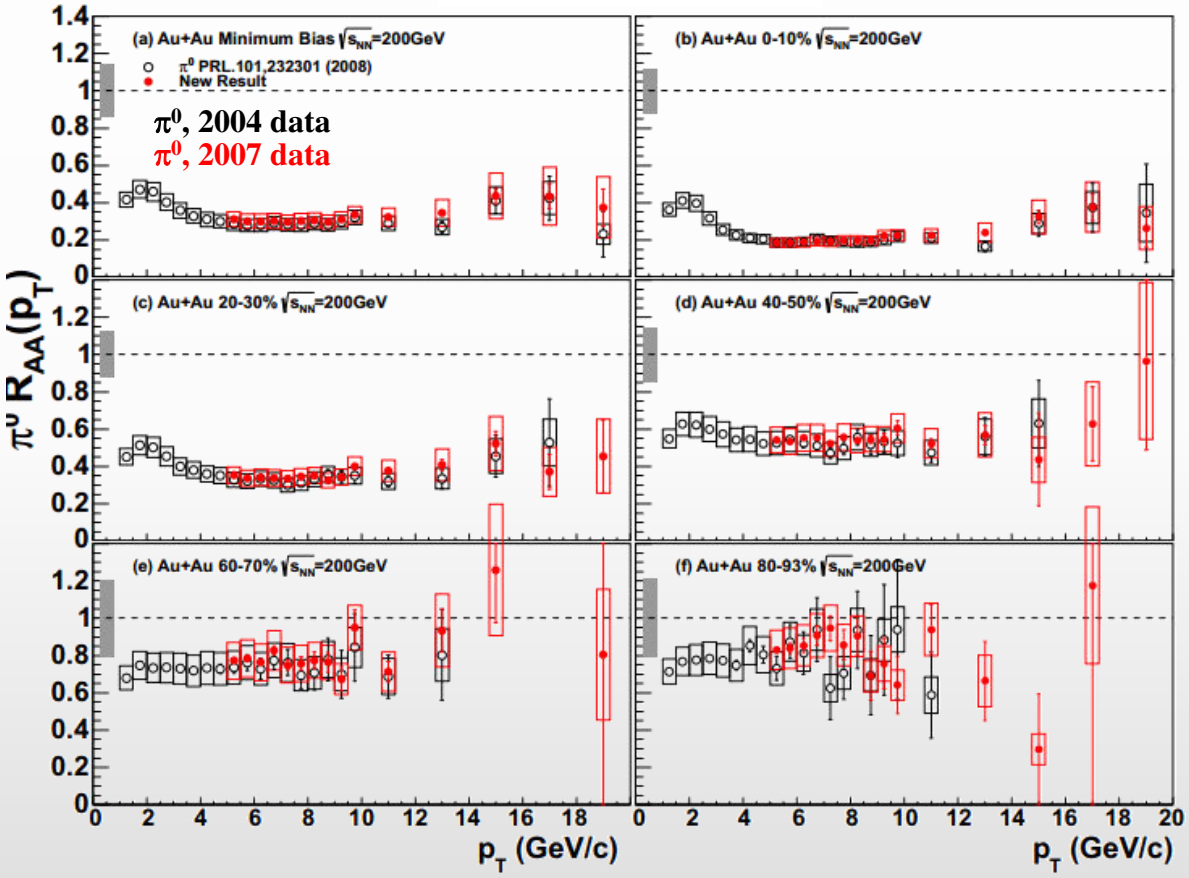

- System size dependence of R_{AA}
- In central collisions suppression is strongest (~ 0.2) at 6-8 GeV/c and decreases at higher/lower momenta
- In peripheral collisions R_{AA} ~ 0.8

R_{AA} << 1 → production of hadrons is suppressed in (semi)central HIC ↔ jet quenching

Model comparison

Parton quenching model (C. Loizides)
hep-ph/0608133v2

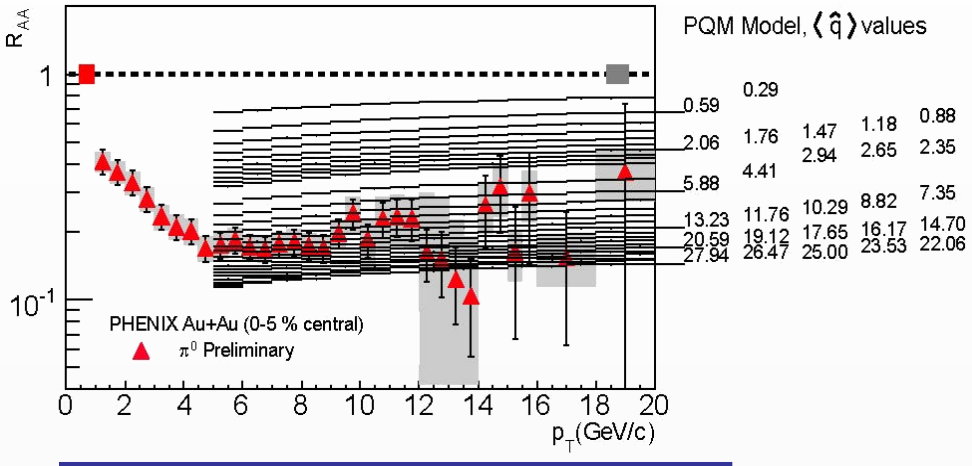

$$6 \le \langle \hat{q} \rangle \le 24 \ \text{ГэВ}^2/\text{фм}$$

GLV (M.Gyulassy, P.Levai, I.Vitev)
nucl-th/0006010v2

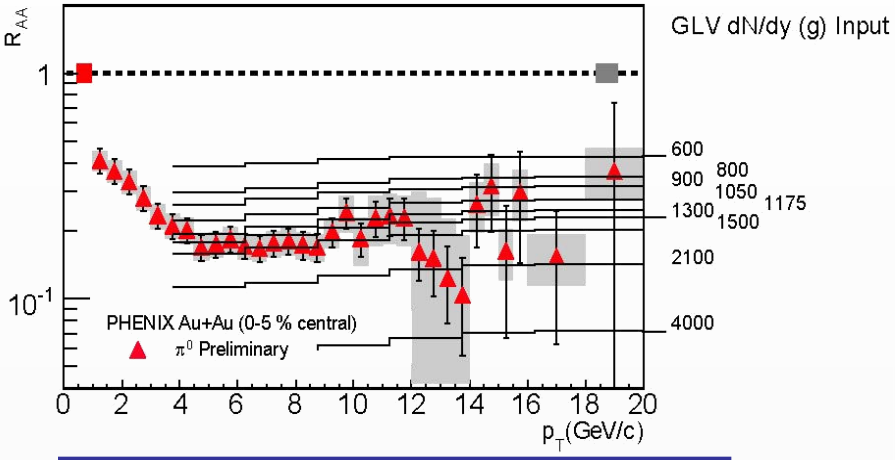

$$1000 \le \frac{dN_g}{dy} \le 2000$$

WHDG (S.Wicks, W.Horowitz, M.Djordjevic, M.Gyulassy)
nucl-th/0512076

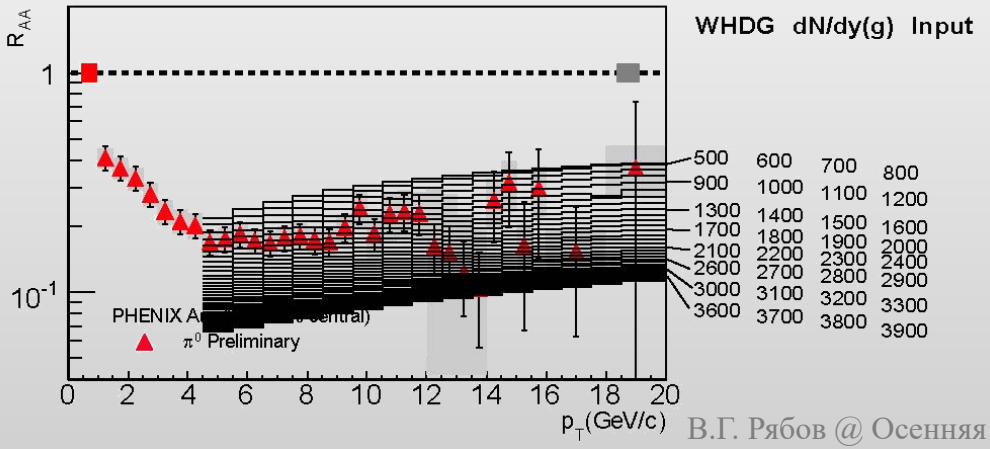

$$600 \le \frac{dN_g}{dy} \le 1600$$

π^0, $R_{AA}(p_T,\varphi)$, Au+Au, $\sqrt{s_{NN}}$ = 200 GeV

Phys. Rev. C 80, 054907 (2009)

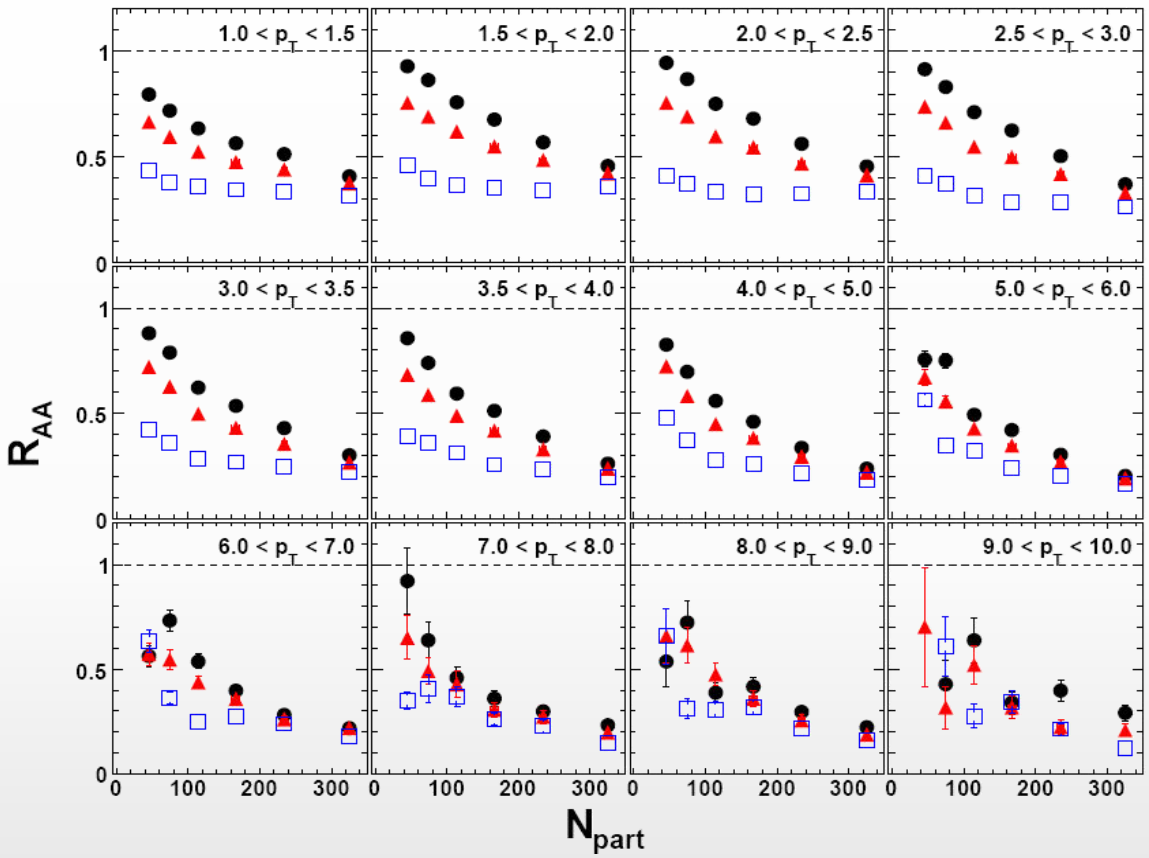

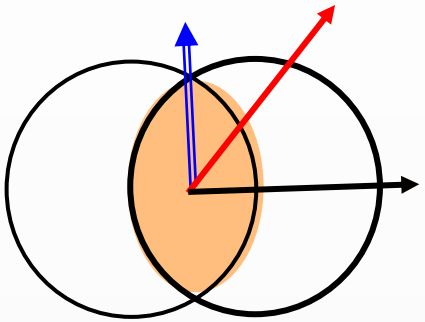

- R_{AA} в плоскости и вне плоскости реакции отличается в ~2 раза

R_{AA} at NICA

- Cross section for hard processes reduces with collision energy → need lots of statistics
- R_{AA} measurements are missing at NICA energies
- STAR provided R_{CP}:

$$R_{CP} = \left\langle N_{coll}^{Peripheral} \right\rangle \cdot dN_{Central} / dy \Big/ \left\langle N_{coll}^{Central} \right\rangle \cdot dN_{Peripheral} / dy$$

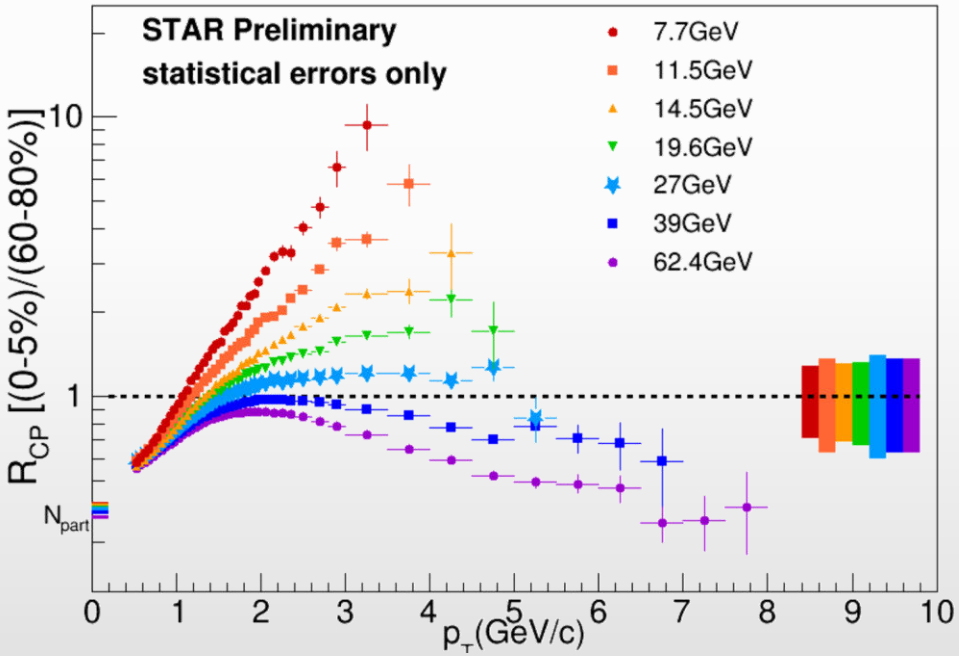

No sign of suppression at $\sqrt{s_{NN}} < 20$ GeV → no jet quenching at NICA energies ???

Need proper measurements to conclude

High-energy heavy-ion reaction data

- Galactic Cosmic Rays composed of nuclei (protons, … up to Fe) and E/A up to 50 GeV
- These high-energy particles create cascades of hundreds of secondary, etc. particles

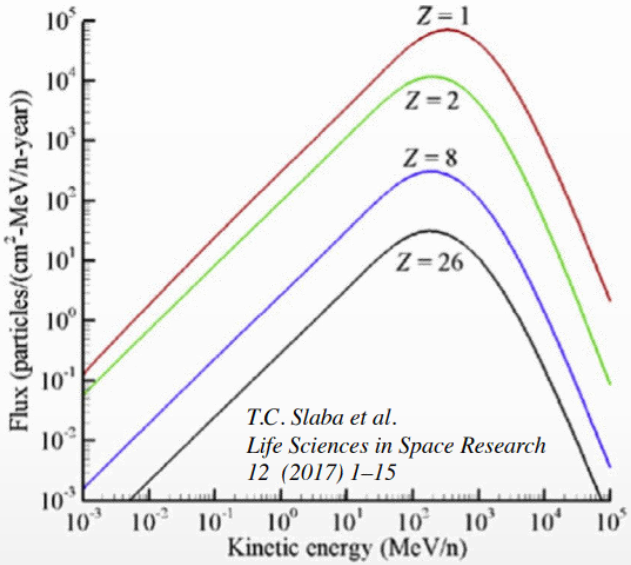

- Cosmic rays are a serious concern to astronauts, electronics, and spacecraft.
- The damage is proportional to Z^2, contribution of secondaries p, d, t, ^{3}He, and ^{4}He is also significant
- Need input information for transport codes for shielding applications (Geant-4, Fluka, PHITS, etc.):
  - ✓ total, elastic/reaction cross section
  - ✓ particle multiplicities and coellecense parameters
  - ✓ outgoing particle distributions: $d^2N/dEd\Omega$

High energy heavy ion reaction data

- NICA can deliver different ion beam species and energies:
  - ✓ Targets of interest (C = astronaut, Si = electronics, Al = spacecraft) + He, C, O, Si, Fe, etc.
- No data exist for projectile energies > 3 GeV/n

dE/dx vs momentum in TPC

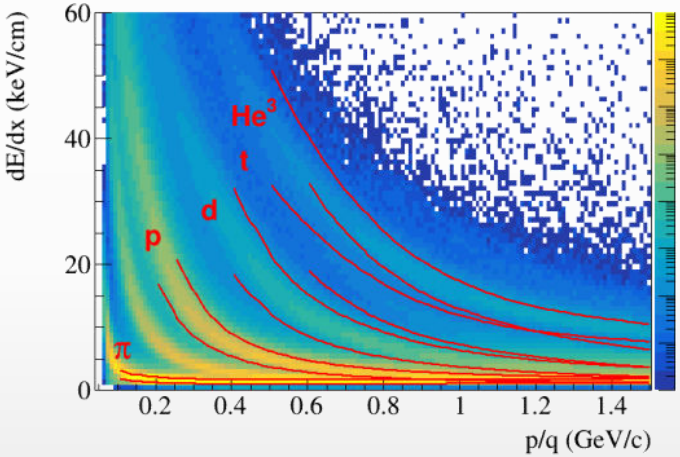

m^2 vs. momentum in TOF

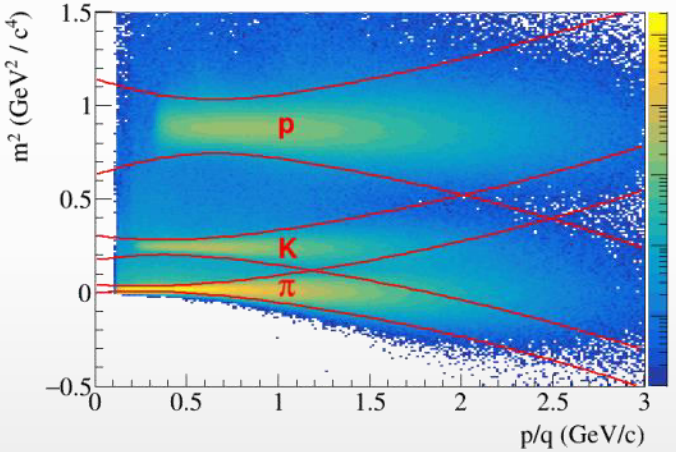

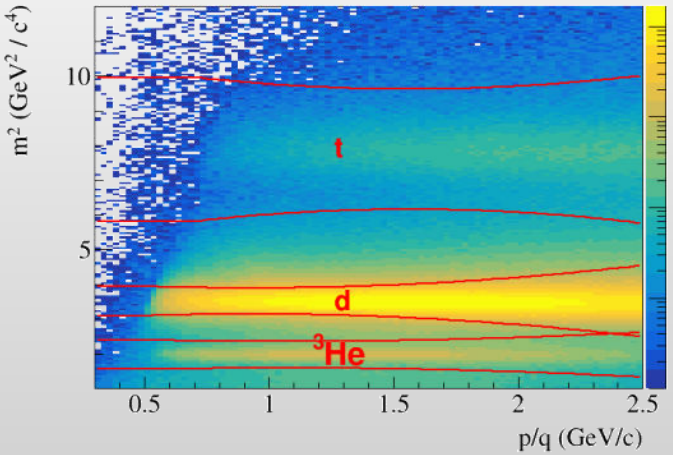

MPD has excellent light fragment identification capabilities in a wide rapidity range → unique capability of the MPD in the NICA energy range

Anisotropic flow at RHIC/LHC - scaling

PoS 2006 (2006) 021

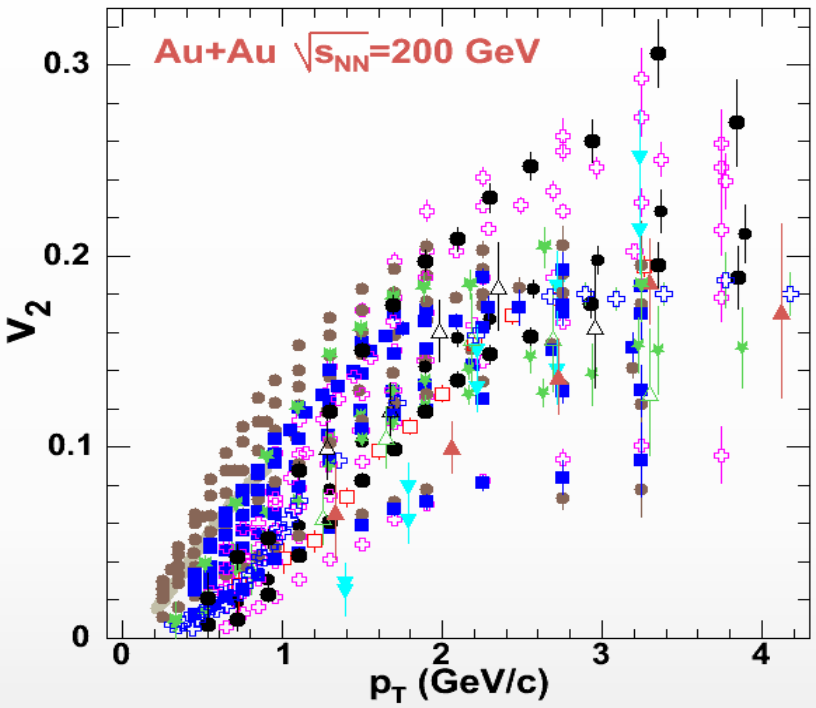

PHENIX (Phys.Rev.Lett.91, Preliminary: QM05, GRC 06)

- $\pi^+ + \pi^-$: min.bias, 0-10%,10-20%,20-30%,30-40%,40-50%,20-60%
- $K^+ + K^-$: min.bias, 0-10%,10-20%,20-30%,30-40%,40-50%,20-60%
- $p + \bar{p}$: min.bias, 0-10%,10-20%,20-30%,30-40%,40-50%,20-60%
- d : min.bias, 10-50%
- ϕ : 20-60%

STAR (Phys. Rev. Lett. 92,Phys. Rev. C 72 (2005), Preliminary QM05, SQM06)

- $\pi^+ + \pi^-$: min.bias
- K^0_S : min.bias, 5-30%,30-70%
- $p + \bar{p}$: min.bias
- $\Lambda + \bar{\Lambda}$: min.bias, 5-30%,30-70%
- $\Xi + \bar{\Xi}$: min.bias
- $\Omega + \bar{\Omega}$: min.bias
- ϕ : min.bias

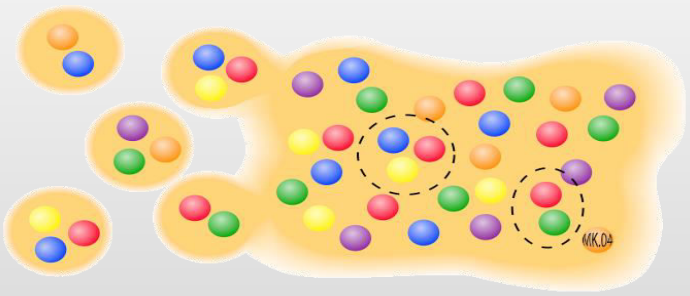

n=2 for mesons and n=3 for baryons

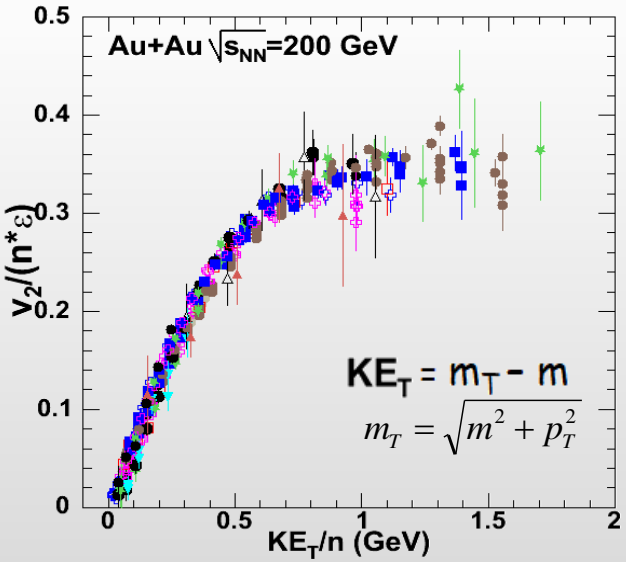

Observed n_q-scaling suggests <u>partonic degrees of freedom</u>

Non-central heavy-ion collisions

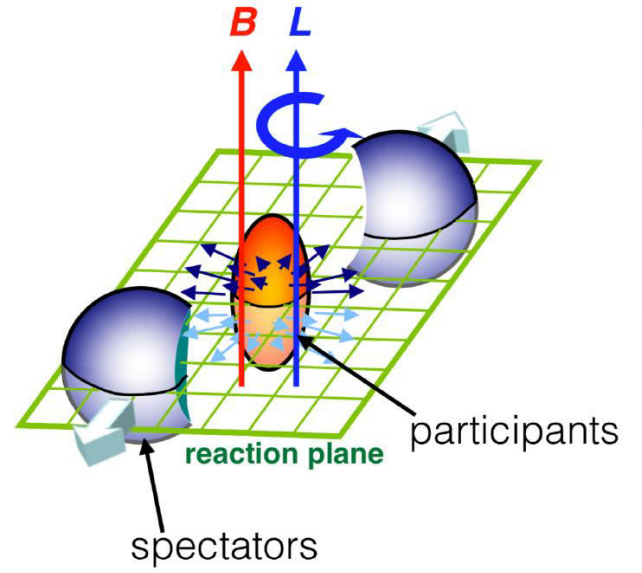

Large angular momentum due to medium rotations (PRC 77 (2008) 024906, Beccattini et al.)

Strong magnetic field (~ 10^{13} T) formed for a short period of time (NPA 803 (2008), Kharzeev et al.)

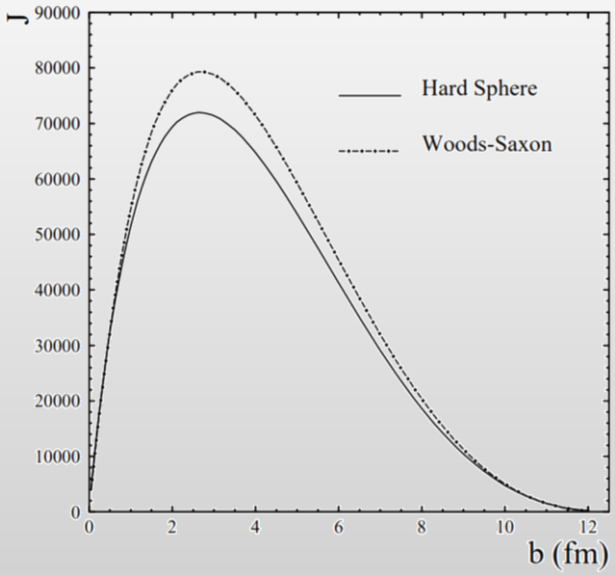

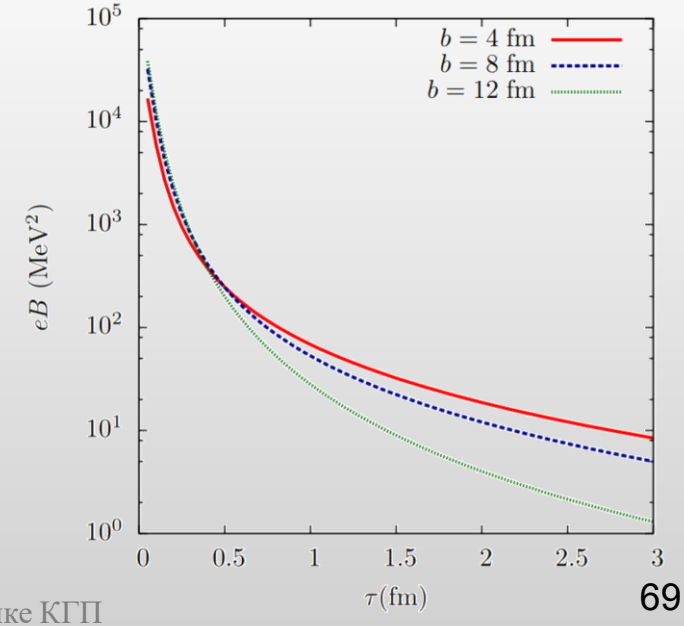

Angular momentum and magnetic field

System	Angular momentum ($h/2\pi$)
Electron in hydrogen atom	$\sqrt{l(l+1)}$
^{132}Ce (highest for nuclei)	70
Heavy-ion collisions	$10^4 - 10^5$

System	Vorticity (s^{-1})
Solar sub-surface	10^{-7}
Terrestrial atmosphere	10^{-5}
Great red spot of Jupiter	10^{-4}
Tornado core	10^{-1}
Heated soap bubbles	100
Turbulent flow in superfluid He	150
Heavy-ion collisions *STAR: Nature 548 (2017) 62*	**10^7 - 10^{21}**

Focus of the study is to see the effect of large angular momentum and magnetic field in heavy-ion collisions

System	Magnetic Field in Tesla
Human brain	10^{-12}
Earth's magnetic field	10^{-5}
Refrigerator magnet	10^{-3}
Loudspeaker magnet	1
Strongest field in lab	10^3
Neutron star	10^6
Heavy-ion collisions	***10^{15} - 10^{16}***

By orders of magnitude exceeds anything existing in the modern Universe

Global hyperon polarization

- Large angular momentum and strong magnetic field formed in mid-central heavy-ion collisions → polarization of particles in the final state

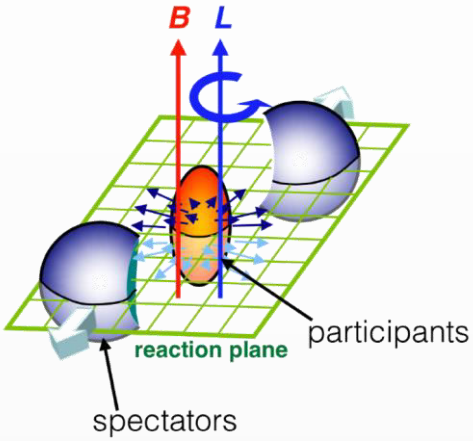

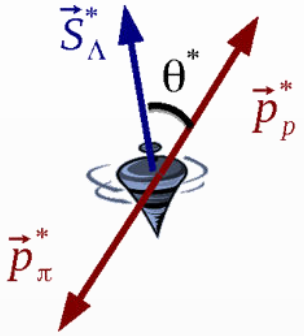

- $\Lambda/\bar{\Lambda}$ are "self-analyzing" probes → preferential emission of proton in in spin direction

STAR, Nature 548, 62 (2017)

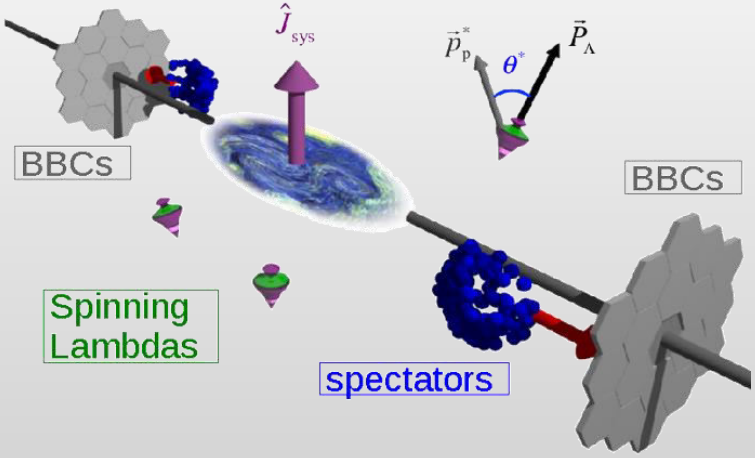

Phys.Rev.Lett.94:102301,2005;
Erratum-ibid.Lett.96:039901,2006

The global polarization observable is defined by [34]:

$$P_\Lambda = \frac{8}{\pi \alpha_\Lambda} \frac{\langle \sin(\Psi_{EP} - \phi^*_p) \rangle}{R_{EP}}. \quad (1)$$

Here $\alpha_\Lambda = 0.732 \pm 0.014$ [35] is the Λ decay parameter, Ψ_{EP} the event plane angle, ϕ^*_p the azimuthal angle of the proton in the Λ rest frame, R_{EP} the resolution of the event plane angle and the brackets $\langle . \rangle$ denote the average

Global hyperon polarization

- Global hyperon polarization measurements in mid-central A+A collisions at $\sqrt{s_{NN}}$= 3-5000 GeV

STAR, Phys.Rev.C, 104(6):L061901, 2021

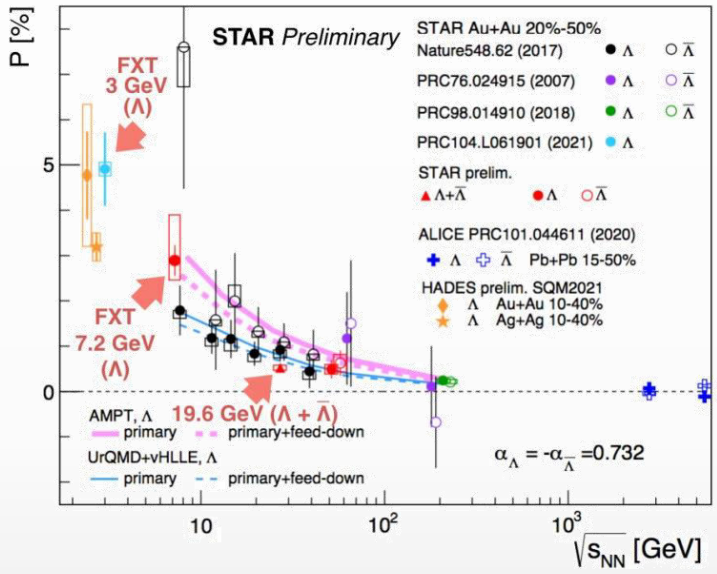

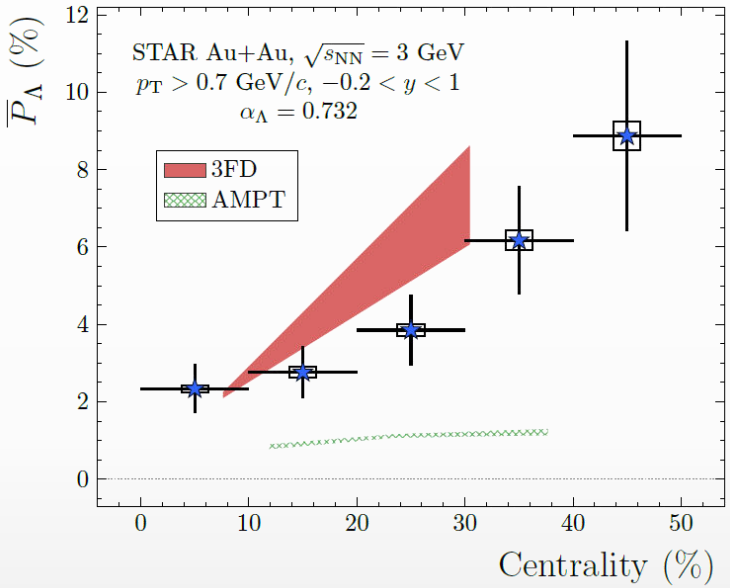

- Global polarization of hyperons experimentally observed, decreases with $\sqrt{s_{NN}}$
- Hint for a Λ-$\bar{\Lambda}$ difference, magnetic field, $P_\Lambda \simeq \frac{1}{2}\frac{\omega}{T} + \frac{\mu_\Lambda B}{T}$, $P_{\bar{\Lambda}} \simeq \frac{1}{2}\frac{\omega}{T} - \frac{\mu_\Lambda B}{T}$?
- Energy dependence of global polarization is reproduced by AMPT, 3FD, UrQMD+vHLLE
- AMPT with partonic transport strongly underestimates measurements at $\sqrt{s_{NN}}$ = 3 GeV → hadron gas?

MPD: extra points in the energy range 4-11 GeV with small uncertainties; centrality, p_T and rapidity dependence of polarization not only for Λ, but other (anti)hyperons (Λ, Σ, Ξ)

Polarization of vector mesons: K*(892) and ϕ

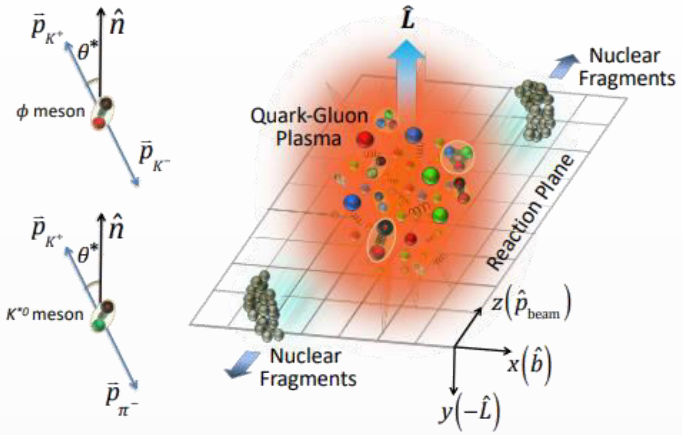

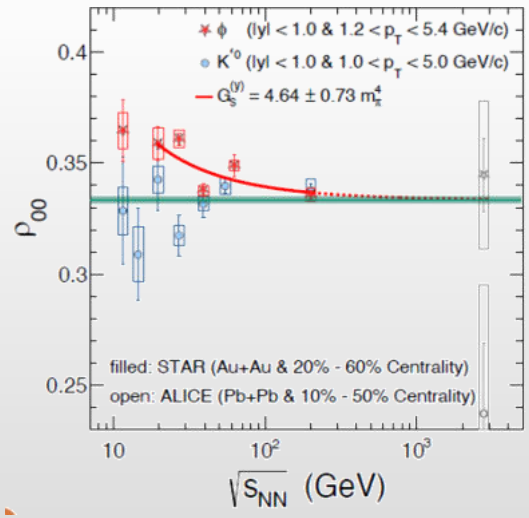

- Light quarks can be polarized by $|\bar{J}|$and $|\bar{B}|$
- If vector mesons are produced via recombination their spin may align
- Quantization axis:
  - ✓ normal to the production plane (momentum of the vector meson and the beam axis)
  - ✓ normal to the event plane (impact parameter and beam axis)
- Measured as anisotropies:

$$\frac{dN}{dcos\theta} = N_0\left[1 - \rho_{0,0} + cos^2\theta\left(3\rho_{0,0} - 1\right)\right]$$

$\rho_{0,0}$ is a probability for vector meson to be in spin state = 0 → $\rho_{0,0}$ = 1/3 corresponds to no spin alignment

- Measurements at RHIC/LHC challenge theoretical understanding → ρ_{00} can depend on multiple physics mechanisms (vorticity, magnetic field, hadronization scenarios, lifetimes and masses of the particles)

MPD: extend measurements in the NICA energy range, $\sqrt{s_{NN}}$ < 11 GeV